1521-0111/101/3/154–167$35.00
MOLECULAR PHARMACOLOGY

dx.doi.org/10.1124/molpharm.121.000415
Mol Pharmacol 101:154–167, March 2022

New Synthetic Caffeine Analogs as Modulators of the Cholinergic System[S]

Camila Fabiani, Brunella Biscussi, Juan P. Munafó, Ana P. Murray, Jeremías Corradi, and Silvia S. Antollini

Instituto de Investigaciones Bioquímicas de Bahía Blanca, Departamento de Biología, Bioquímica y Farmacia, (C.F., J.P.M., J.C., S.S.A.) and Instituto de Química del Sur, Departamento de Química, (B.B., A.P.M.), Universidad Nacional del Sur y Consejo Nacional de Investigaciones Científicas y Técnicas

Received September 22, 2021; accepted December 26, 2021

ABSTRACT

Alzheimer's disease is a multifactorial neurodegenerative disorder. Since cholinergic deficit is a major factor in this disease, two molecular targets for its treatment are the acetylcholinesterase (AChE) and the nicotinic acetylcholine receptors (nAChRs). Given that caffeine is a natural compound that behaves as an AChE inhibitor and as a partial agonist of nAChRs, the aim of this work was to synthetize more potent bifunctional caffeine analogs that modulate these two molecular targets. To this end, a theophylline structure was connected to a pyrrolidine structure through a methylene chain of different lengths (3 to 7 carbon atoms) to give compounds **7**–**11**. All caffeine derivatives inhibited the AChE, of which compound **11** showed the strongest effect. Electrophysiological studies showed that all compounds behave as agonists of the muscle and the neuronal α7 nAChR with greater potency than caffeine. To explore whether the different analogs could affect the nAChR conformational state, the nAChR conformational-sensitive probe crystal violet (CrV) was used. Compounds **9** and **10** conduced the nAChR to a different conformational state comparable with a control nAChR desensitized state. Finally, molecular docking experiments showed that all derivatives interacted with both the catalytic and anionic sites of AChE and with the orthosteric binding site of the nAChR. Thus, the new synthetized compounds can inhibit the AChE and activate muscle and α7 nAChRs with greater potency than caffeine, which suggests that they could be useful leaders for the development of new therapies for the treatment of different neurologic diseases.

SIGNIFICANCE STATEMENT

In this work we synthetized caffeine derivatives which can inhibit acetylcholinesterase and activate both muscle and α7 nicotinic acetylcholine receptors (nAChRs) with higher potency than caffeine. These analogs can be divided into two groups: a non-desensitizing and a desensitizing nAChR group. From the nAChR non-desensitizing group, we propose compound **11** as the most interesting analog for further studies since it inhibits acetylcholinesterase with the highest potency and activates the nAChRs in the picomolar range without inducing receptor desensitization.

Introduction

Alzheimer's disease (AD), the most prevalent neurodegenerative disorder in the elderly, is mainly characterized by progressive cognitive decline. The rationale for the *cholinergic hypothesis* of AD (Davies and Maloney, 1976; Perry et al., 1981; Contestabile, 2011; Hampel et al., 2018) is that there is a decrease in the total amount of acetylcholine receptors (AChRs) because of the progressive death of cholinergic neurons (Whitehouse et al., 1986; Paterson and Nordberg, 2000; Ma and Qian, 2019). Since the loss of cognitive functions is strongly correlated with a disruption in the cholinergic neurotransmission, an enhancement of this neurotransmission either by inhibition of the acetylcholinesterase (AChE) or potentiation of the nicotinic acetylcholine receptors (nAChRs) could improve memory and cognition (Craig et al., 2011).

The AChE is the enzyme that terminates the acetylcholine (ACh) signal at the postsynaptic membrane. The inhibition of this enzyme therefore increases the amount of ACh that can bind to the nAChRs. The AChE active cavity involves two sites: the catalytic site (CAS), which consists of two "subsites" (the anionic subsite which arranges the substrate in a suitable orientation, and the ester subsite which is responsible for the catalytic action of the enzyme) and the peripheral anionic site (PAS), a region that is an important target for interaction with different molecules, among which are the amyloid peptides (Inestrosa et al., 2005). Current pharmacological agents, such as tacrine, donepezil, rivastigmine, and

This work was supported by CONICET (Grant PIP 11220170100399C to SSA), Agencia Nacional de Promoción Científica y Tecnológica (ANPCyT) (Grant PICT 2017-1443 to APM), and Universidad Nacional del Sur (Grants PGI 24/B282 to SSA and PGI 24/B279 to JC).

No author has an actual or perceived conflict of interest with the contents of this article.

dx.doi.org/10.1124/molpharm.121.000415.

[S] This article has supplemental material available at molpharm.aspetjournals.org.

ABBREVIATIONS: AChE, acetylcholinesterase; AChR, acetylcholine receptor; AD, Alzheimer's disease; BBE, best binding energy; ^{13}C, carbon-13; carb, carbamylcholine; CAS, catalytic site; $CDCl_3$, chloroform-d; CrV, crystal violet; DMF, dimethylformamide; HEPES, 4-(2-hydroxyethyl)-1-piperazineethanesulfonic acid; ^{1}H, hydrogen-1; KD, dissociation constant; nAChR, nicotinic acetylcholine receptor; PAS, peripheral anionic site; PNU, PNU-120596 = N-(5-Chloro-2 = 4- dimethoxyphenyl)-N'-(5-methyl-3-isoxazolyl)-urea; R, resting state.

galantamine, are used to inhibit AChE (Martorana et al., 2010). Unfortunately, these drugs can alleviate the symptoms of AD but are unable to prevent disease progression (Selkoe, 2012; Singh et al., 2013).

Other interesting molecular targets for the treatment of AD are the nAChRs. They are integral membrane pentameric proteins that belong to the Cys-loop family of ligand-gated ion channels (Karlin and Akabas, 1995; Le Novère and Changeux, 1995). These receptors contain an extracellular domain, which carries the binding site, a transmembrane region, formed by four transmembrane segments from each subunit (M1–M4), and an intracellular region that contains sites for receptor modulation and determinants of channel conductance (Corradi and Bouzat, 2016; Morales-Perez et al., 2016). The binding of its natural agonist, ACh, triggers a conformational change that ends in the opening of the ion channel and the flux of positive ions across the membrane, causing membrane depolarization (McKay et al., 2007; Pohanka, 2012; Corradi and Bouzat, 2016).

In vertebrates, seventeen nAChR subunits combine to yield a great variety of receptors. Muscle nAChRs, which have been the model for biophysical and pharmacological studies of the nicotinic receptor family, are heteropentameric receptors formed by the combination of two $\alpha 1$ subunits and one of each β, ε, and δ subunit. The homomeric $\alpha 7$ and the $\alpha 4\beta 2$ neuronal receptors are the most abundant nAChRs in the mammalian brain. These receptors are widely dispersed throughout the central nervous system, and their unique distribution within the structures involved in cognition implicates them as important potential targets for neurodegenerative diseases. The most vulnerable neurons in AD are those expressing high levels of $\alpha 7$ neuronal nAChRs (Dani and Bertrand, 2007) being that the reason why $\alpha 7$ receptor is the most implicated and studied in the mentioned disease, as well as in other neurologic disorders such as Parkinson's disease and schizophrenia (D'Andrea and Nagele, 2006; Dani and Bertrand, 2007), and has emerged as a potential therapeutic target (Pohanka, 2012).

Although a great effort has been made to develop specific drugs to potentiate nAChRs, nowadays AChE inhibition is the only approved treatment to slow the symptoms of mild to moderate AD. Commercial AChE inhibitors are considered indirect nAChR agonists that locally increase endogenous neurotransmitter levels. Thus, much effort is put on the design of multitarget drugs that can both inhibit AChE and directly improve nAChR function. In a previous work (Fabiani et al., 2018), we confirmed that caffeine inhibits AChE activity and demonstrated that it is an agonist of nAChRs, thus becoming an interesting lead compound for the design of new molecules.

The aim of this work was to obtain more potent caffeine analogs. We synthetized five compounds using as initial substrates theophylline, which bears similarity to caffeine, and pyrrolidine, whose structure is present in nicotine's molecule. We here demonstrate that the synthetized compounds behave as bifunctional drugs that can inhibit the AChE and activate nAChRs with higher potency than caffeine.

Materials and Methods

Torpedo californica specimens obtained from the Pacific coast of California (Aquatic Research Consulants, San Pedro, CA, USA) were killed by pithing, and the electric organs were dissected and stored at -70°C until use.

All the chemicals employed were of the best available grade (Aldrich, Merck) and were used without further purification. AChE from *electric eel* (type VI-S), 5,5′-dithiobis(2- nitrobenzoic acid), acetylthiocholine iodide, tacrine, crystal violet (CrV), and all other drugs were obtained from Sigma Aldrich. PNU-120596 [N-(5-Chloro-2,4-dimethoxyphenyl)-N0-(5-methyl-3-isoxazolyl)-urea] (PNU) was obtained from Tocris Biosciences (Bristol, UK).

Synthesis of Caffeine Analogs

General Chemistry. Hydrogen-1 (^{1}H) and carbon-13 (^{13}C) nuclear magnetic resonance (NMR) spectra, including two-dimensional correlation spectroscopy, heteronuclear single quantum coherence, and heteronuclear multiple bond correlation experiments were recorded on a Bruker Avance ARX-300 spectrophotometer at room temperature in chloroform-d ($CDCl_3$). Chemical shifts (δ) are reported in ppm from tetramethylsilane (TMS, δ= 0.00 ppm). All melting points (mps) were determined using a Reichert melting points apparatus.

Column chromatography was carried out with Merck silica gel 60 (0.2–0.63 mm, 240–400 mesh). The progress of the reactions was controlled using silica gel-60 F 254 chromatofoils (Merck). The development of thin layer chromatograms was performed by visualization with UV light of wavelengths 254 and 366 nm and/or in *p*-anisaldehyde developing stain.

Microwave assisted reactions were performed in a microwave reactor CEM Discover Benchmate oven (CEM Corp, Matthews, North Carolina, USA).

All derivatives were rigorously characterized by NMR spectroscopy. For new compounds, copies of ^{1}H, ^{13}C, distortionless enhancement by polarization, and heteronuclear single quantum coherence NMR graphical spectra are also provided (Supplemental Figures 1–14).

General Procedure for the Synthesis of Compounds 2–6. To a solution of compound **1** (0.1802 g, 1.0 mmol) and anhydrous potassium carbonate (K_2CO_3, 207 mg, 1.5 mmol) in dry dimethylformamide (1 ml), the corresponding α,ω-dibromoalkane was added (2 mmol). The solution was placed in a 10-ml closed system microwave vessel with a magnetic stirrer and was irradiated for 10 minutes at 80°C with the following fixed conditions: standard mode, 150W, 5-minute heating ramp to reach working temperature, medium stirring, max. power off. The solvent was subsequently removed by addition of distilled H_2O (3 ml) and extraction with ethyl acetate (3 × 2 ml). The organic phase was dried over anh. Na_2SO_4, filtered and the solvent was evaporated to afford the desired product. The residue was purified by column chromatography on silica gel 60 (70–230 mesh) with dichlomethane/methanol (90:10) to afford the desired ether (yields of 31 to 42%).

7-(3-bromopropyl)-1,3-dimethyl-3,7-dihydro-1H-purine-2,6-dione (2). Compound **1** was treated with 1,3-dibromopropane (204 μl) according to the general procedure to yield compound **2** as a white solid (43% yield); mp: 133–135°C. ^{1}H NMR (300 MHz, $CDCl_3$, ppm) δ 7.64 (*s*, 1H), 4.47 (*t*, *J*= 6.5 Hz, 2H), 3.60 (*s,* 3H), 3.41 (*s*, 3H), 3.33 (*t*, *J*= 6.0 Hz, 2H), 2.46 (*p*, *J*= 6.3 Hz, 2H); ^{13}C NMR (75 MHz, $CDCl_3$, ppm) δ 155.2, 151.8, 149.4, 141.6, 106.8, 45.4, 32.7, 29.9, 29.6, 28.1.

7-(4-bromobutyl)-1,3-dimethyl-3,7-dihydro-1H-purine-2,6-dione (3). Compound **1** was treated with 1,4-dibromobutane (280 μL) according to the general procedure to yield compound **3** as a white solid (32% yield). ^{1}H NMR (300 MHz, $CDCl_3$, ppm) δ 7.65 (s, 1H), 4.36 (*t*, *J*= 7.1 Hz, 2H), 3.59 (s, 3H), 3.44 (*m,* 2H), 3.41 (s, 3H), 2.08 (*p*, *J*= 6.9 Hz, 2H), 1.90 (*p*, *J*= 6.4 Hz, 2H); ^{13}C NMR (75 MHz, $CDCl_3$, ppm) δ 155.0, 151.5, 148.8, 140.7, 106.8, 46.3, 32.4, 29.8, 29.6, 29.3, 28.8.

7-(5-bromopentyl)-1,3-dimethyl-3,7-dihydro-1H-purine-2,6-dione (4). Compound **1** was treated with 1,5-dibromopentane (275 μL) according to the general procedure to yield compound **4** as a white solid (34% yield); mp: 83–85°C. ^{1}H NMR (300 MHz, $CDCl_3$, ppm) δ 7.56 (s, 1H), 4.30 (*t*, J= 7.2 Hz, 2H), 3.59 (s, 3H), 3.41 (s, 3H), 3.42 (*m*, 2H), 2.02 – 1.83 (*m,* 4H), 1.49 (*p*, J= 6.4 Hz, 2H); ^{13}C NMR (75 MHz, $CDCl_3$,

ppm) δ 155.2, 151.8, 149.1, 140.9, 106.8, 47.1, 33.3, 32.0, 30.1, 29.9, 28.1, 25.0.

7-(6-bromohexyl)-1,3-dimethyl-3,7-dihydro-1H-purine-2,6-dione (5). Compound **1** was treated with 1,6-dibromohexane (310 μl) according to the general procedure to yield compound **5** as a white solid (32% yield). ^{1}H NMR (300 MHz, $CDCl_3$, ppm) δ 7.54 (*s*, 1H), 4.29 (*t*, J= 7.2 Hz, 2H), 3.59 (*s*, 3H), 3.41 (*s*, 3H), 3.38 (*m*, 2H), 196–1.80 (*m*, 4H), 1.58–1.42 (*m*, 2H), 1.43–1.27 (*m*, 2H); ^{13}C NMR (75 MHz, $CDCl_3$, ppm) δ 155.2, 151.8, 149.1, 140.9, 107.1, 47.2, 33.6, 32.5, 30.8, 29.9, 28.1, 27.6, 25.6.

7-(7-bromoheptyl)-1,3-dimethyl-3,7-dihydro-1H-purine-2,6-dione (6). Compound **1** was treated with 1,7-dibromoheptane (342 μl) according to the general procedure to yield compound **6** as a white solid (40% yield); mp: 84–86°C. ^{1}H NMR (300 MHz, $CDCl_3$, ppm) δ 7.55 (*s*, 1H), 4.29 (*t*, J= 7.2 Hz, 2H), 3.59 (*s*, 3H), 3.41 (*s*, 3H), 3.38 (*m*, 2H), 196–1.78 (*m*, 4H), 1.49–1.30 (*m*, 6H); ^{13}C NMR (75 MHz, $CDCl_3$, ppm) δ 155.2, 151.8, 149.0, 140.9, 107.1, 47.3, 33.8, 32.5, 30.9, 29.9, 28.2, 28.1, 28.0, 26.3.

General Procedure for the Synthesis of Compounds 7–11. To a solution of **2-6** (0.1 mmol) in dry dimethylformamide (DMF) (1 ml), pyrrolidine (0.3 mmol) was added. The reaction mixture was placed in a microwave-special closed vial and irradiated for 5–12 minutes at 100°C (150 W) until the disappearance of the starting compound was detected by TLC. The solvent was subsequently removed by adding distilled H_2O (2 m) and extracting with ethyl acetate (3 × 2 ml). The organic phase was dried over anh. Sodium sulfate was filtered and evaporated under vacuum to afford the desired product (yields 50 to 70%).

1,3-dimethyl-7-(3-(pyrrolidin-1-yl)propyl)-3,7-dihydro-1H-purine-2,6-dione (7). Intermediate **2** (0.239 mmol, 0.0723 g) was treated with pyrrolidine (0.76 mmol, 62.8 μl) following the general procedure. The reaction mixture was irradiated for 5 minutes at 100°C (150 W). The desired product **7** was obtained as a pale yellow solid (70%); mp: 55-56°C. ^{1}H NMR (300 MHz, $CDCl_3$, ppm) δ 7.60 (*s*, 1H), 4.39 (*t*, J= 6.5 Hz, 2H), 3.59 (*s*, 3H),3.41 (*s*, 3H), 2.52–2.44 (*m*, 4H), 2.40 (*t*, J= 6.8 Hz, 2H), 2.05 (*p*, J= 6.7 Hz, 2H), 1.78 (*p*, J= 3.1 Hz, 4H). ^{13}C NMR (75 MHz, $CDCl_3$, ppm) δ 155.1, 151.7, 148.9, 141.6, 106.9, 53.9, 52.1, 45.1, 29.7, 29.4, 28.0, 23.5.

1,3-dimethyl-7-(4-(pyrrolidin-1-yl)butyl)-3,7-dihydro-1H-purine-2,6-dione (8). Intermediate **3** (0.25 mmol, 0.0803 g) was treated with pyrrolidine (0.76 mmol, 62.8 μl) following the general procedure. The reaction mixture was irradiated for 10 minutes at 100°C (150 W). The desired product **8** was obtained as a brown oil (65%). ^{1}H NMR (300 MHz, $CDCl_3$, ppm) δ 7.56 (*s*, 1H), 4.32 (*t*, J= 6.5 Hz, 2H), 3.59 (*s*, 3H), 3.41 (*s*, 3H), 2.47 (*p*, J= 7.5 Hz, 6H), 1.93 (*p*, J= 7.4 Hz, 2H), 1.77 (*p*, J= 3.1 Hz, 4H) 1.54 (*p*, J= 7.6 Hz, 2H). ^{13}C NMR (75 MHz, $CDCl_3$, ppm) δ 155.2, 151.8, 149.0, 140.9, 107.1, 55.8, 54.3, 47.2, 29.8, 29.2, 28.1, 25.9, 23.5.

1,3-dimethyl-7-(5-(pyrrolidin-1-yl)pentyl)-3,7-dihydro-1H-purine-2,6-dione (9). Intermediate **4** (0.096 mmol, 0.0317 g) was treated with pyrrolidine (0.29 mmol, 24.6 μl) following the general procedure. The reaction mixture was irradiated for 10 minutes at 100°C (150 W). The desired product **9** was obtained as a brown oil (47%). ^{1}H NMR (300 MHz, $CDCl_3$, ppm) δ 7.55 (*s*, 1H), 4.29 (*t*, J= 7.1 Hz, 2H), 3.59 (*s*, 3H),3.41 (*s*, 3H), 2.55 – 2.48 (*m*, 4H), 2.48–2.41 (*m*, 2H), 1.91 (*p*, J= 7.4 Hz, 2H), 1.79 (*p*, J= 3.1 Hz, 4H) 1.58 (*p*, J= 7.5 Hz, 2H), 1.36 (*q*, J= 7.6 Hz, 2H). ^{13}C NMR (75 MHz, $CDCl_3$, ppm) δ 155.2, 151.8, 149.0, 140.9, 107.1, 56.3, 54.3, 47.3, 30.9, 29.8, 28.4, 28.1, 24.5, 23.5 (t).

1,3-dimethyl-7-(6-(pyrrolidin-1-yl)hexyl)-3,7-dihydro-1H-purine-2,6-dione (10). Intermediate **5** (0.067 mmol, 0.023 g) was treated with pyrrolidine (0.2 mmol, 16.3 μl) following the general procedure. The reaction mixture was irradiated for 10 minutes at 100°C (150 W). The desired product **10** was obtained as a brown oil (72%). ^{1}H NMR (300 MHz, $CDCl_3$, ppm) δ7.54 (*s*, 1H), 4.28 (*t*, J= 7.0 Hz, 2H), 3.59 (*s*, 3H), 3.41 (*s*, 3H), 2.59–2.49 (*m*, 4H), 2.45 (*t*, J= 7.5 Hz, 2H), 1.88 (*p*, J= 6.3 Hz, 2H), 1.80 (*p*. J= 3.1 Hz, 4H), 1.53 (*p*, J= 7.4 Hz, 2H), 1.44–1.29 (*m*, 4H). ^{13}C NMR (75 MHz, $CDCl_3$, ppm) δ 155.2, 151.8, 149.1, 140.9, 107.1, 56.4, 54.3, 47.3, 30.9, 29.9, 28.7, 28.1, 27.1, 26.4, 23.5.

1,3-dimethyl-7-(7-(pyrrolidin-1-yl)heptyl)-3,7-dihydro-1H-purine-2,6-dione (11). Intermediate **6** (0.10 mmol, 0.036 g) was treated with pyrrolidine (0.3 mmol, 24.6 μl) following the general procedure. The reaction mixture was irradiated for 12 minutes at 80°C (150 W). The desired product **11** was obtained as a brown oil (45%). ^{1}H NMR (300 MHz, $CDCl_3$, ppm) δ 7.53 (*s*, 1H), 4.28 (*t*, J= 7.1 Hz, 2H), 3.59 (*s*, 3H), 3.41 (*s*, 3H), 2.58–2.48 (*m*, 4H), 2.44(*t*, J= 7.5 Hz, 2H), 1.87 (*os*, 2H), 1.79 (*os*, 4H), 1.53 (*p*, J= 6.6 Hz, 2H), 1.39–1.27 (*m*, 6H). ^{13}C NMR (75 MHz, $CDCl_3$, ppm) δ 155.2, 151.8, 149.0, 140.9, 107.1, 56.5, 54.3, 47.4, 30.9, 29.9, 29.0, 28.8, 28.1, 27.6, 26.4, 23.5.

In Vitro AChE Activity. *Electric eel* AChE was used as source of cholinesterase. Inhibitory activity on AChE was determined in vitro by the spectrophotometric method developed by Ellman with slight modifications (Ellman et al., 1961). Buffer phosphate A (8 mM K_2HPO_4, 2.3 mM NaH_2PO_4) and B (8 mM K_2HPO_4, 2.3 mM NaH_2PO_4, 0.15 M NaCl, 0.05% Tween 20, pH 7.6) were used for the dilutions. The lyophilized enzyme, 500 U of AChE, was dissolved in buffer phosphate A to obtain 5 U/ml of stock solution. For each bioassay, the enzyme was diluted with buffer phosphate B to produce 0.126 U/ml of enzyme solution. Samples (500-0.01 μM) were dissolved in buffer phosphate B, with MeOH (2.5%) added as a cosolvent. Finally, the enzyme solution (300 μl) and sample solution (300 μl) were mixed in a test tube and incubated at room temperature for 60 minutes. The reaction was initiated by adding 600 μl of the substrate solution (0.5 mM of 5′5'-dithio-bis(2-nitrobenzoic acid), 0.6 mM of acetylthiocholine iodide, 0.1 M of Na_2HPO_4, pH 7.5). Absorbance was read at 405 nm for 120 seconds at 25°C (JASCO V-630BIO Spectrophotometer equipped with an EHCS-760 Peltier; Tokyo, Japan). Enzyme activity was measured by comparing reaction rates for the samples to the blank. Tacrine (99%) was used as the reference inhibitor. All the experiments were performed in triplicate. IC_{50} values were determined with the aid of GraphPad Prism 5 software.

nAChR-rich Membranes Preparation. nAChR-rich membrane fragments were prepared from *Torpedo californica* electric tissue as described previously (Barrantes, 1982). Briefly, electric tissue was chopped into small pieces, homogenized using a Virtis homogenizer under controlled conditions, and submitted to a series of centrifugation steps to obtain *T. californica* crude membranes, ending in a high-speed sucrose gradient centrifugation. The middle fraction obtained corresponds to nAChR-rich membranes with a specific activity of the order of 1.0–1.5 nmol of α-BTX sites/mg of protein (Barrantes, 1982).

Cell Culture. Human embryonic kidney 293 cells were transfected with mouse α, β, δ and ε subunits, for muscle, or human α7 and Ric-3 subunits, for neuronal nAChR expression, as was previously described (Bouzat et al., 1994; daCosta, et al., 2011). Each receptor cDNA subunit was sub-cloned into pRBG4 plasmid for heterologous expression. For electrophysiological measurements, a plasmid encoding green fluorescent protein (GFP) was included in all transfections to allow the identification of transfected cells under fluorescence optics.

nAChR Conformational State Characterization. nAChR-rich membranes were resuspended in buffer A (150 mM of NaCl, 0.25 mM of $MgCl_2$, and 20 mM of HEPES buffer, pH 7.4) at a final concentration of 100 μg of protein/ml. nAChR conformational changes were analyzed using crystal violet (CrV) as described previously (Fabiani et al., 2018). nAChR-rich membranes resuspended in buffer A were incubated for 15 min with pyrrolidine, theophylline, or the caffeine analogs **7-11**. For the measurements conducted with nAChR in the desensitized state, *T. californica* membranes were afterwards incubated with 1 mM of carbamylcholine (carb) for 15 min. The membranes were subsequently titrated with increasing concentrations of CrV (in buffer A). After each addition of CrV, the samples were incubated for 15 min before obtaining the fluorescence emission spectra. CrV was excited at 600 nm, and the fluorescence

emission spectra were collected from 605–700 nm. Fluorimetric measurements were performed in 2-ml quartz cuvettes in a SLM model 4800 fluorimeter (SLM Instruments, Urbana, IL) using a vertically polarized light beam from Hannovia 200-W mercury/xenon arc obtained with a Glan-Thompson polarizer (4-nm excitation and emission slits). To determine the CrV dissociation constants (K_D), the values of CrV maximum fluorescence emission were plotted as a function of the logarithmic CrV concentrations (M). The resulting sigmoid curve was fitted to the Boltzmann function, and K_D was calculated.

Electrophysiological Experiments. HEK293 cells expressing muscle or neuronal nAChRs were used for single-channel measurements two days after transfection. Single-channel recordings were performed in the cell-attached patch-clamp configuration at room temperature (20°C) and at -70 mV of membrane potential. The bath and pipette solutions contained 142 mM of KCl, 5.4 mM of NaCl, 1.8 mM of $CaCl_2$, 1.7 mM of $MgCl_2$, and 10 mM of HEPES (pH 7.4). Either ACh or the tested compounds (pyrrolidine, theophylline, or caffeine analogs **7-11**) were added to the pipette solution. Single-channel currents were recorded using an Axopatch 200B patch-clamp amplifier (Molecular Devices), digitized at 200 kHz and low-pass filtered at a cutoff frequency of 10 kHz using a computer interface Instrutech ITC-18 (HEKA Instruments, Inc.). Single-channel events were idealized by the half amplitude threshold criterion using the program QuB 2.0.0.28 (www.qub.buffalo.edu) with a digital low-pass filter at 9 kHz for muscle and α7 nAChR recordings, or 3 kHz for α7 recordings obtained in the presence of PNU. The open and closed durations were estimated from the idealized recordings by the maximum interval likelihood (MIL) function in QuB (Qin et al., 1996) with a dead time of 0.03 millisecond for muscle, or 0.1 millisecond for α7 receptor. The analysis was performed on the basis of a kinetic model whose probability density function curves properly described the corresponding histograms following the maximum likelihood criteria. For muscle nAChR, the best fitting was obtained with the classic kinetic model previously reported (Bouzat et al., 1994; Corradi et al., 2007). For α7 recordings, the analysis was performed by sequentially adding an open and/or closed state to a starting C↔O model until it properly describes the corresponding duration histograms (Fabiani et al., 2018; Lasala et al., 2019). In general, for α7 recordings obtained in the presence of ACh or each of the testing compounds plus PNU, the best description was obtained when the model contained five or six closed states and two or three open states, similar to that previously described (Fabiani et al., 2018; Lasala et al., 2019). Clusters were identified as a series of closely separated openings preceded and followed by closings longer than a critical duration. Critical closed times were calculated by MIL between each closed component. Typically, critical time between the second and third closed components for muscle (~15 milliseconds) and between the third and fourth closed components for α7 nAChRs (~60 milliseconds) were selected in QuB to chop the idealized data and create a sub-data set that only contained clusters to define mean cluster duration and open probability within clusters (Popen). Popen within clusters was determined by calculating the mean fraction of time that the channel is open within a cluster.

Molecular Modeling. Homology models of the extracellular domain of the mouse α1/δ and α1/ε nAChR interfaces were created using as template either the structure of the chimera α7/acetylcholine binding protein which contains the loop C partially closed and which was crystallized with the partial agonist lobeline (PDB code 5AFM), or the structure of the human $\alpha 4\beta 2$ nicotinic receptor in complex with nicotine, which contains the loop C closed (PDB code 5KXI, Morales-Perez et al., 2016). The amino acid sequences were aligned using ClustalW (http://www.ebi.ac.uk/Tools/msa/clustalw2/), and modeling was performed using Modeler 9.19 (Sali et al., 1995). Ten models were generated for each interface, of which the one with the lowest energy, calculated by Modeler as the discreet optimized protein energy score (Shen and Sali, 2006), and the smallest percentage of amino acids in the disallowed region of the Ramachandran plot, obtained with Procheck (Laskowski et al., 1993), was selected for docking studies.

Molecular Docking. For molecular docking, we used the modeled mouse nAChR interfaces and the human AChE structure obtained from the PDB Data Bank (PDB code 4EY7, Cheung et al., 2012). Ligands were designed with Avogadro 1.2.0 and docked using AutoDock4.2 (Morris et al., 2009) The grid was defined around the orthosteric binding site for the nAChR models, and in the CAS/PAS site for the AChE structure. A hundred genetic algorithm runs were performed for each condition. Clustering of the results was done with AutoDock on the basis of a root-mean-square deviation cut-off of 2.0 Å. To evaluate the ability of each receptor to bind agonist, we compared the best binding energy (BBE) and the frequency of conformations that bind the agonist in the correct orientation in the binding pocket. Docking results were corroborated in at least three different procedures, and the most representative docking result was plotted with Discovery Studio Visualizer 2021 (Dassault Systèmes BIOVIA Corp, San Diego, USA).

Data Analysis. In electrophysiological experiments, comparison of two mean values were performed through unpaired Student's t test, whereas in fluorescence experiments, comparison of more than two mean values were realized by analysis of variance (randomized one-way ANOVA), followed by post hoc test analysis of multiple comparisons Bonferroni. Differences were considered significant at $P < 0.05$ and highly significant at $P < 0.01$. In the case of $n = 3$, the data were considered if the coefficient of variation (standard deviation/mean) was < 0.1.

Results

Synthesis of Caffeine Analogs. In the present work, we focused on obtaining caffeine derivatives that could enhance cholinergic transmission with greater potency and efficacy than the lead compound. To potentiate caffeine activity, we combined two molecular entities, caffeine and nicotine, which have the same molecular targets (Fig. 1). Nicotine, the principal alkaloid of the tobacco plant, is an agonist of both neuronal and muscle nAChR (Akk and Auerbach, 1999; Fu et al., 2009; Carlson and Kraus, 2020) and also behaves as an inhibitor of the AChE (Ijomone and Nwoha, 2015). It is a bicyclic molecule formed by an N-methyl substituted pyrrolidine, protonated at physiologic pH, mimicking the quaternary ammonium of the ACh, and a pyridine group with high electron density, mimicking the acetic group of the ACh. Along with the well-known harmful effects attributed to nicotine (Mishra et al., 2015; Mackenbach et al., 2017), some beneficial health effects were also described, mainly in memory and cognition processes (Jarvik, 1991; Rusted et al., 2005; Alhowail, 2021; Barreto et al., 2015; Gandelman et al., 2018),

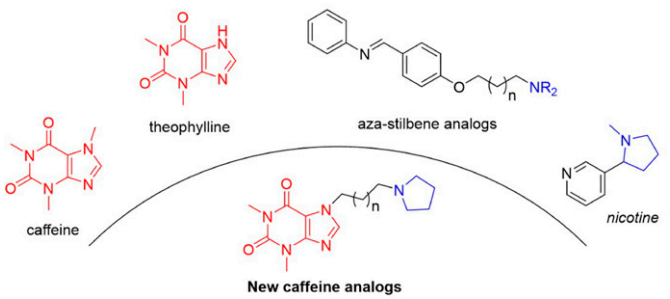

Fig. 1. Acetylcholinesterase inhibitors and nicotinic acetylcholine receptor agonist (nicotine), base structures for the design of new caffeine analogs as acetylcholinesterase inhibitors and nicotinic acetylcholine receptor modulators.

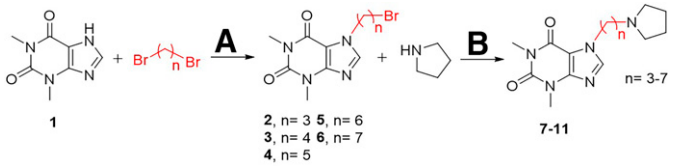

Scheme 1. Synthesis of derivatives **7–11.** (A) anh. Potassium carbonate, dry dimethylformamide, microwave; (B) dry dimethylformamide, microwave.

and some studies suggested that it could be useful for the treatment of AD (Srivareerat et al., 2009; Guo et al., 2015). To synthetize caffeine analogs, we used theophylline, a structure similar to caffeine but without the methyl group in position N-7. A pyrrolidine group, which is present in nicotine structure, was connected to N-7 of theophylline by means of a methylene chain with different length. This allowed us to obtain five compounds (from 3 to 7 methylene groups, referred to as compounds **7** to **11**, respectively) (Fig. 1).

The general synthesis for the novel compounds **7–11** is depicted in Scheme 1. In a first step, the reaction between theophylline, **1**, with the corresponding dibromoalkane in K_2CO_3/dry DMF, was carried out to offer intermediates **2–6** in moderate yields which presented a side chain of variable length (3 to 7 methylenes). The reaction was carried out in a microwave reactor under the following conditions: 150 W, 100°C, 10 minutes. Compounds **2–6** were subsequently treated with pyrrolidine in dry DMF, also in a microwave-assisted reaction (150 W, 100°C, 5–12 minutes), to obtain caffeine derivatives **7–11** with good yields (Scheme 1).

Inhibition of Acetylcholinesterase by Caffeine Analogs. The ability of caffeine derivatives to inhibit the AChE was analyzed and compared with that of the natural alkaloid, caffeine, and of their chemical precursors, theophylline and pyrrolidine.

We initially analyzed the inhibition of AChE activity in the presence of theophylline or pyrrolidine. We observed that pyrrolidine did not affect AChE activity at any concentration tested (50–500 μM). On the other hand, theophylline inhibited the enzymatic activity, similar to that we reported for caffeine but with about one-fifth the potency (Table 1). As a reference compound, we analyzed the inhibition of AChE activity by tacrine, a potent AChE inhibitor (Biscussi et al., 2020).

Based on the IC_{50} values shown in Table 1, the potency of each compound was higher than theophylline, pyrrolidine, and caffeine. The IC_{50} values for compounds **7** and **11** were about 8.5- and 2150-fold, respectively, lower than for theophylline, which suggested that the length of the linker (n in Scheme 1) that connects theophylline with pyrrolidine is crucial for the inhibition of the enzyme.

TABLE 1
Inhibition of cholinesterase activity by compounds 7–11 and their corresponding precursors. Tacrine was tested as a control of acetylcholinesterase inhibition. ND= not detected.

Compound	IC_{50} (μM)	log IC_{50} ± SD
Theophylline	473.0	2.675 ± 0.0787
Pyrrolidine	ND	
Caffeine	87.0	1.939 ± 0.0562
Compound 7	56.2	1.750 ± 0.0310
Compound 8	21.8	1.337 ± 0.0442
Compound 9	13.5	1.130 ± 0.0259
Compound 10	6.1	0.7849 ± 0.0447
Compound 11	0.22	−0.6655 ± 0.0593
Tacrine	0.029	−1.53 ± 0.05

Muscle Nicotinic Acetylcholine Receptor Activation by Caffeine Derivatives. Given that caffeine acts as a partial agonist and an open-channel blocker of the nAChR (Fabiani et al., 2018), we here analyzed the effect of caffeine analogs on the muscle nAChR using the patch-clamp technique. In the presence of 30 μM of ACh, receptor activation was observed as events of 5.2 ± 0.6 pA (at -70 mV of membrane potential) grouped in clusters of 140 ± 70 millisecond with a Popen of 0.4 ± 0.1 (Fig. 2). In the presence of either compounds **7–11** or their corresponding precursors (theophylline and pyrrolidine), single-channel events were observed, thus indicating that these drugs act as muscle nAChR agonists (Fig. 2).

To study the kinetics of muscle nAChR activation in the presence of each compound, we recorded single-channel events at a range of concentrations, from 0.01 pM to 30 μM. For all the synthetic analogs, receptor activation was elicited at drug concentrations (about 0.01–0.1 pM) lower than that we previously reported for caffeine (10 μM, Fabiani et al., 2018). At all concentrations of all compounds, nAChR activation was elicited as isolated openings without the ability to coalesce in clusters, as shown in the example of compound **9** (Fig. 3).

After idealization, we obtained the corresponding open- and closed-duration histograms. For ACh, open time histograms were described by two components whose durations and relative areas were similar to those reported previously (Bouzat et al., 2000; Corradi et al., 2007). Closed time histograms were described by three or four components, the two briefest corresponding to closings within clusters.

For compound **9,** the open duration remained constant at concentrations lower than 30 μM (Fig. 3). The mean durations

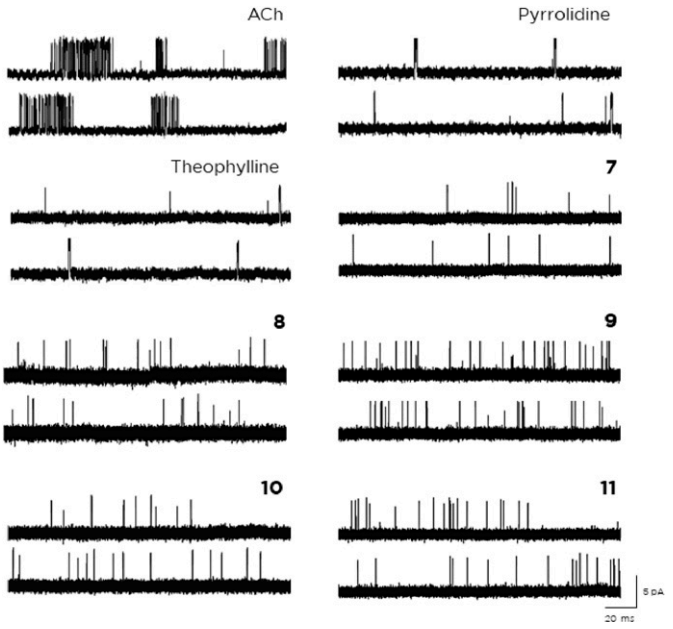

Fig. 2. Activation of the muscle nicotinic acetylcholine receptor by the synthetized caffeine analogs **7–11**. Single-channel events elicited by 30 μM of acetylcholine or 10 μM of pyrrolidine, theophylline, and each compound. Openings were recorded at -70 mV of membrane potential, and they are shown as upward deflections.

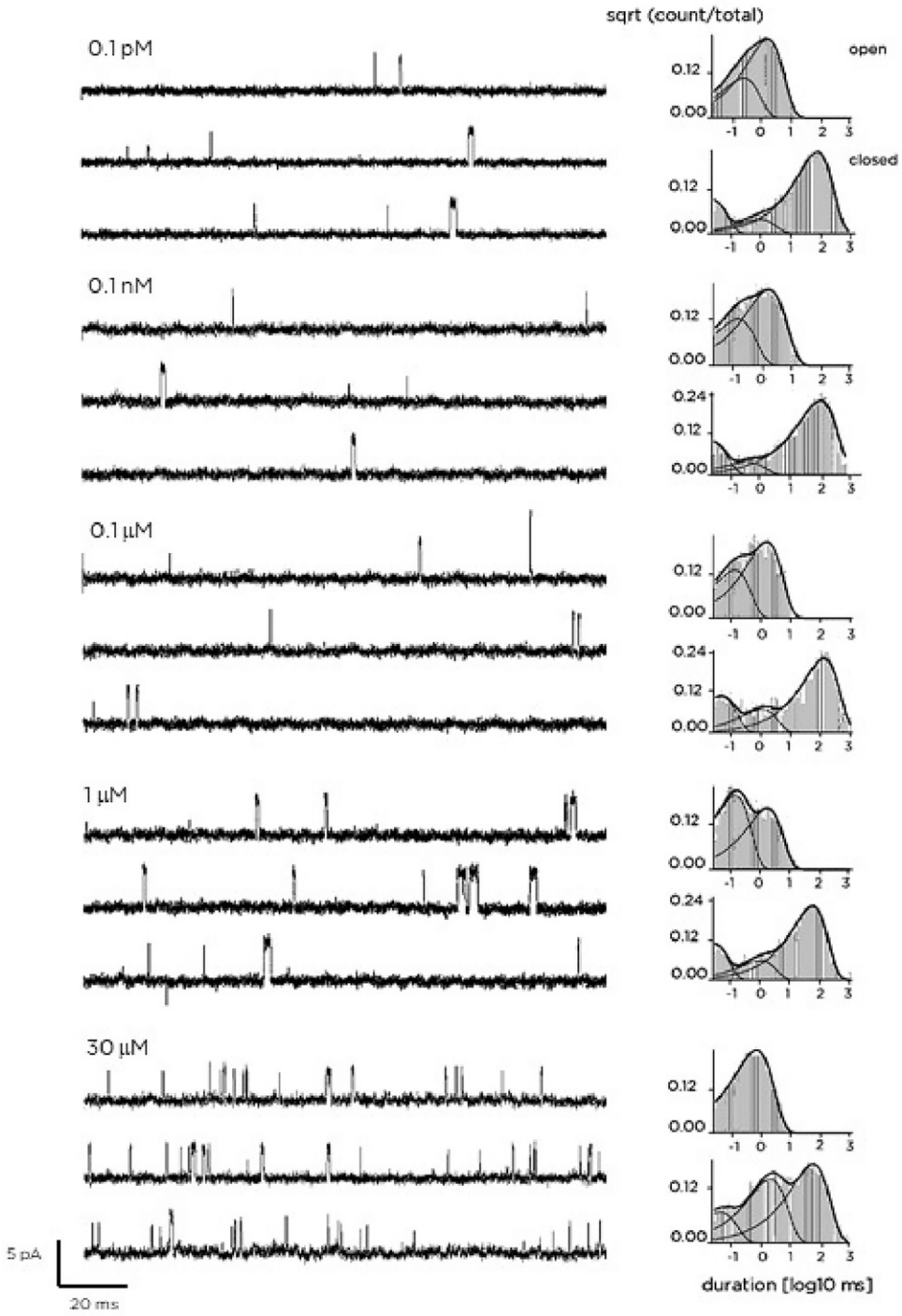

Fig. 3. Activation profile of muscle nicotinic acetylcholine receptor at various concentrations of compound **9**. Openings were recorded at -70 mV of membrane potential and they are shown as upward deflections. On the right of each trace are the open- (*top*) and closed-duration histograms (*bottom*) obtained for each condition.

for the longest open component were 1.36 ± 0.28 milliseconds for 30 μM of ACh (n = 8) and 1.26 ± 0.09 milliseconds (n = 17) for compound **9** at 0.1–10 μM (P = 0.13; comparison of mean values was performed using Student t test). At compound **9** concentrations equal to or higher than 30 μM, the open duration was reduced as shown in Fig. 3. The mean open time was 0.52 ± 0.01 milliseconds (n = 3), which was different from that obtained for 30 μM of ACh (n = 8), (P = 0.00036; comparison of mean values was performed using Student t test). This reduction in the mean open time may suggest that compound **9** also behaves as a muscle nAChR open-channel blocker, similarly to that we previously reported for caffeine (Fabiani et al., 2018).

All these results demonstrate that the synthetized compounds behave as partial agonists of the muscle nAChR with greater potency than caffeine.

Neuronal Nicotinic Acetylcholine Receptor Activation by Caffeine Derivatives. To determine if caffeine derivatives can also activate neuronal nAChRs, we performed complementary experiments to study the effect of compound **9** on the neuronal human α7 nAChR.

When α7 nAChR was activated by 100 μM of ACh, single-channel events appeared as brief isolated openings with a maximum amplitude of about 10 pA (at -70 mV of membrane potential) as reported previously (Fig. 4, Bouzat et al., 2008). Compound **9** at 10 or 100 μM, in the absence of ACh, elicited the typical brief and isolated α7 channel openings (Fig. 4). To further confirm that the observed openings were due to α7 activation, we performed single-channel recordings in the presence of PNU-120596.

PNU-120596 is a type II positive allosteric modulator (PAM) of α7 nAChR, which enhances the probability of agonist-elicited channel opening and agonist-induced open-channel durations and also reduces desensitization. In the absence of an agonist, PNU-120596 cannot induce channel activation (Hurst et al., 2005; DaCosta et al., 2011; Bouzat et al., 2018). It has been extensively used as a tool to reveal α7 channel activity because it increases open probability and produces activation in long clusters at the single-channel level (Lasala et al., 2019). Thus, in the presence of 100 μM of ACh and 1 μM of PNU, α7 activation appeared as long clusters of about 3065 ± 1728 milliseconds, similar to that previously reported (daCosta et al., 2011).

In the presence of 10 μM of compound **9** and 1 μM of PNU, the expected long clusters of openings were readily detected, with a mean cluster duration of 2629 ± 1615 milliseconds (n = 8), thus confirming that this compound is an agonist of α7 nAChR (Fig. 4). Clusters showed a lower open probability compared with that obtained in the presence of ACh (0.61 ± 0.02 (n = 8) and 0.91 ± 0.03 (n = 6), respectively, P = 0.00095, comparison of mean values was performed using Student t test), which indicates that this compound activates α7 receptors with lower efficacy than ACh, or with the same efficacy but also produces an additional block.

Given that we previously demonstrated that caffeine activates α7 at concentrations higher than 300 μM in the absence of PNU (Fabiani et al., 2018), our results confirm that compound **9**, as a representative of all caffeine derivatives, behaves as an α7 agonist with higher potency than caffeine.

nAChR Conformational Changes Induced by Caffeine Analogs. Since we previously demonstrated that caffeine behaves both as a partial agonist and negative modulator of nAChRs (Fabiani et al., 2018) and that this behavior correlates with distinct nAChR conformational states, we here extended our study to the conformational states of the nAChR in the presence of theophylline, pyrrolidine and compounds **7–11**. To this end, we used the fluorescence probe crystal violet, an open channel blocker of the nAChR, which presents a higher affinity for the desensitized (D) state with respect to the resting (R) one (Lurtz and Pedersen, 1999). Thus, in this experiment, we studied the nAChR under two different situations: i) the nAChR in the absence of carb, to observe if the analogs induce any conformational change, and ii) the nAChR in the presence of desensitizing concentrations of carb, to check if the compounds alter the response of nAChR to carb. The difference between the K_D values obtained with a sample before and after incubation

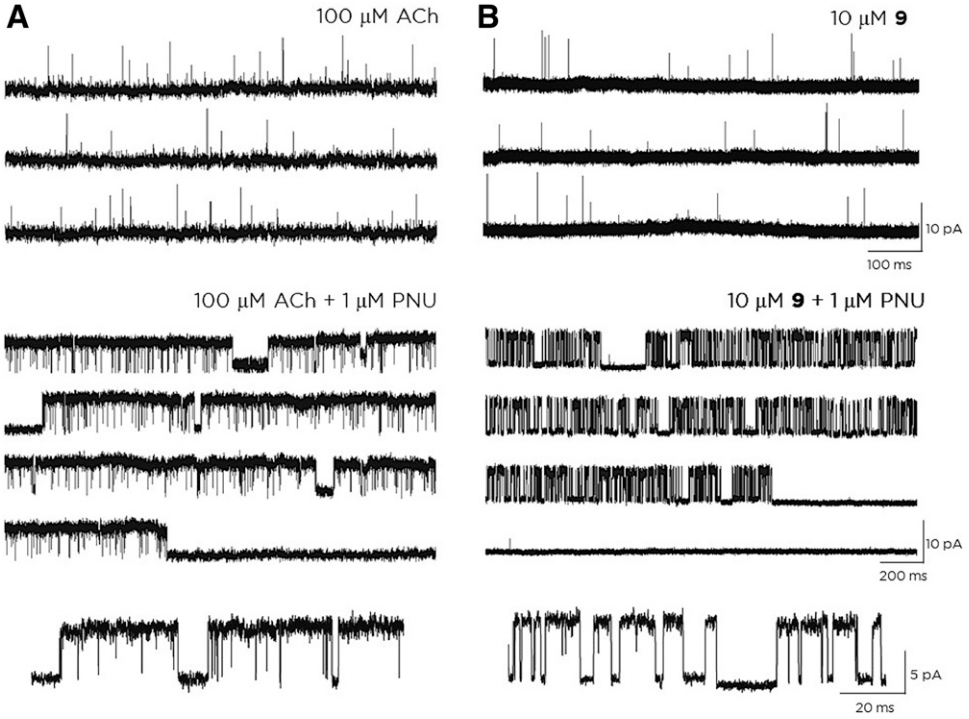

Fig. 4. Neuronal α7 receptor activation by synthetized compounds. (A) Single-channel events obtained from cells transfected with human α7 receptor and activated by 100 μM of acetylcholine in the absence (*top*) or presence (*bottom*) of 1 μM of PNU-120596, N-(5-Chloro-2,4- dimethoxyphenyl)-N'-(5-methyl-3-isoxazolyl)-urea. (B) Similar events were elicited by 10 μM of compound **9**. Events were obtained from cell-attached configuration at -70 mV membrane potential in the absence (*top*) or presence (*bottom*) of 1 μM of PNU-120596, N-(5-Chloro-2,4- dimethoxyphenyl)-N'-(5-methyl-3-isoxazolyl)-urea.

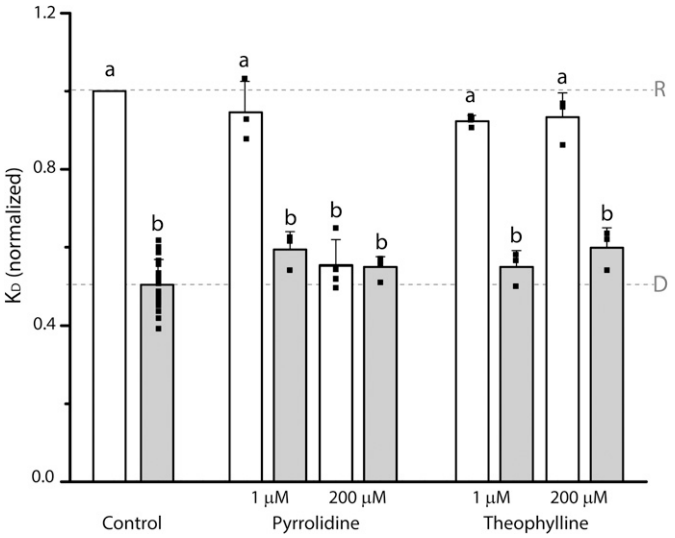

Fig. 5. Dissociation constant values of crystal violet in the absence and presence of carbamylcholine (white and gray columns, respectively) obtained in a control condition or after incubation with two different concentrations of pyrrolidine and theophylline. The dotted lines show the crystal violet dissociation constant values for the receptor in resting (R) and desensitized (D) states. Changes in dissociation constant were calculated with respect to the resting state "R" of the nicotinic acetylcholine receptor in the control condition. Each column represents the mean ± SD of the total number of samples at each condition. Each data point is also shown. The comparisons were done between each experimental condition and the control condition without carbamylcholine ("R" state) using randomized one-way ANOVA. Means from conditions sharing a letter (a or b) are not statistically different, while different letters denote highly significant differences ($P < 0.01$).

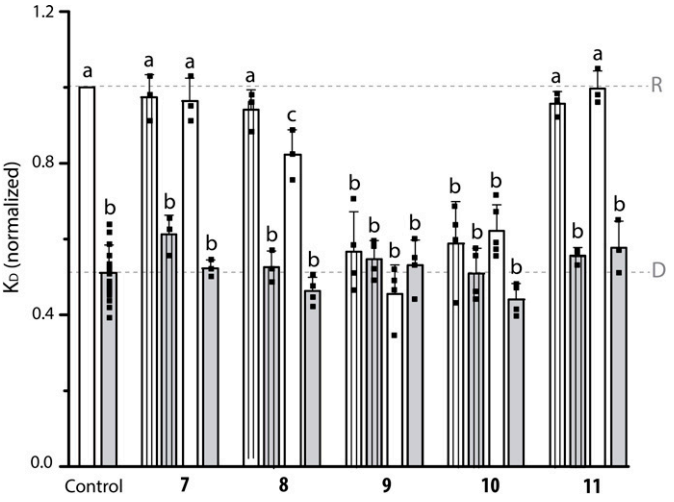

Fig. 6. Dissociation constant values of crystal violet in the absence and presence of carbamylcholine (white and gray columns, respectively) obtained before (control condition) or after incubation with two different concentrations (1 μM, lined pattern columns and 200 μM, empty columns) of compounds **7–11**. The dotted lines show the crystal violet dissociation constant values for the receptor in resting (R) and desensitized (D) states. Changes in dissociation constant were calculated with respect to the resting state "R" of the nicotinic acetylcholine receptor in the control condition. Each column represents the mean ± SD of the total number of samples at each condition. Each data point is also shown. The comparisons were done between each experimental condition and the control condition without carbamylcholine ("R" state) using randomized one-way ANOVA. Means from conditions sharing a letter (a, b, or c) are not statistically different, while different letters denote highly significant differences ($P < 0.01$).

with the agonist carb is not only directly indicative of nAChR conformational changes but also indirectly indicative of nAChR functionality (Fabiani et al., 2018).

The incubation of nAChR-rich membranes from *T. californica* with theophylline at low ($n = 4$) and high ($n = 4$) concentrations induced no changes on the conformational state of the nAChR: K_D values in the absence and presence of carb were similar to the K_D values obtained from a control condition in the absence ($n = 8$) and presence ($n = 8$) of carb, respectively (Fig. 5). In contrast, the presence of pyrrolidine at low ($n = 4$) and high ($n = 4$) concentrations induced changes on the nAChR conformational state at concentrations of 200 μM or higher. Under these conditions, the K_D values obtained in the absence of carb were close to the ones obtained for the nAChR in the desensitized state, suggesting that high concentrations of pyrrolidine lead to receptor desensitization (Fig. 5).

To explore whether the activation of the nAChR could be correlated with its conformational changes, we incubated nAChR-rich membranes from *T. californica* with increasing concentrations (from 0.01 pM to 400 μM) of compounds **7–11** in the absence and in the presence of carb (Fig. 6). We observed that in the presence of carb and the analogs, nAChR desensitization occurred and the K_D values were similar in all cases. In the absence of carb, different results were observed for the synthetic compounds. When membranes were incubated with compound **7** ($n = 4$) and **11** ($n = 3$), no changes were observed even at high concentrations. Under these conditions, the K_D values were similar to those obtained in the absence of carb in the control condition, which corresponds to the resting state (Fig. 6). With respect to compound **8** ($n = 3$), high concentrations (200 μM) were needed to provoke a conformational change of the receptor, being this new conformation in between a resting and a desensitized state. When *T. californica* membranes were incubated with compounds **9** ($n = 4$) or **10** ($n = 4$), a decrease in the K_D values was observed. With these compounds, the K_D values obtained at all the tested concentrations were the same as the ones obtained in the presence of carb (Fig. 6). Thus, based on our observations, compounds **9** and **10** provoke receptor desensitization even at very low concentrations (0.01 pM).

Binding Modes of Caffeine Derivatives into the AChE and nAChR. To test potential interactions that each compound can make with the AChE and the nAChR, we performed molecular docking studies. We first analyzed the interaction of each compound on the AChE using the structure 4EY7.pdb crystalized in complex with donepezil (Supplemental Figure 15, Cheung et al., 2012). The AChE structure shows donepezil bound to the active site with its benzyl group located in the CAS and the dimethoxyindanone ring placed in the PAS. Therefore, for our docking studies, we limited the grid dimensions to cover the CAS and PAS regions (CAS/PAS site, Fig. 7A).

We first docked donepezil in the CAS/PAS site as an internal control. The main conformation showed a BBE of about −11.88 Kcal/mol and similar interactions to those reported in the crystal structure (Fig. 7B, Table 2, Cheung et al., 2012). We observed a cation–π interaction between the positive charge of the piperidine group of donepezil and residues D74

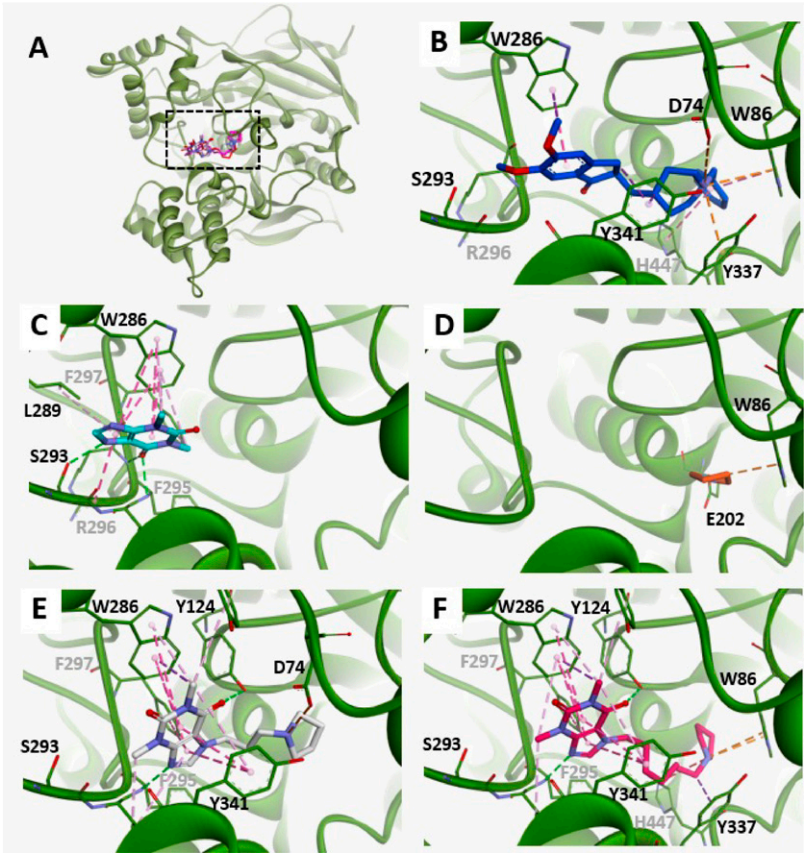

Fig. 7. Molecular docking of various compounds into the catalytic site/peripheral anionic site of the human acetylcholinesterase. (A) Representation as ribbons of the human acetylcholinesterase (PDB code 4EY7) with the best conformation of compounds **7–11** bound. A detailed view of the region indicated with the black square (dashed lines) is shown for donepezil (B), theophylline (C), pyrrolidine (D), compound **7** (E), and compound **11** (F) with their corresponding interactions as dashed lines. Cation-π is shown in orange, π-alkyl in pink, π-π in purple and H-bond in green.

and Y337, π-π staking between the benzyl group and residues W86 and H447, and between the dimethoxyindanone group and residues W286 and Y341, and H-bond between the dimethoxyindanone group and residue F295 (Fig. 7B). Most of these interactions were previously reported as critical for AChE inhibition (Cheung et al., 2012; de Almeida et al., 2018).

We then studied the orientation of pyrrolidine and theophylline in the CAS/PAS site of the human AChE. Our results showed that these molecules can bind in this active site with

TABLE 2

Binding energy and interacting residues. The best binding energy (BBE) of the most stable conformation obtained after docking analyses is shown for each ligand. All the interacting residues observed in the different conformations are listed for each ligand. Residues reported as relevant for enzymatic activity are shown with asterisks (*) or in bold (with residues from the catalytic site indicated with asterisks and from the peripheral anionic site indicated with bold). Data correspond to three independent docking experiments.

Ligand	BBE ± SD (Kcal/mol)	Interacting Residues						
ACh	−4.91 ± 0.11	W86*	G122	S203*	R296	F338*	H447*	
		G121	E202	F295	Y337	**Y341**		
Donepezil	−11.88 ± 0.24	**D74**	**Y124**	S293	R296	**Y341**		
		W86*	**W286**	F295	Y337	H447*		
Theophylline	−5.31 ± 0.02	**Y72**	L289	V294	R296	F338*		
		W286	S293	F295	F297	**Y341**		
Pyrrolidine	−4.78 ± 0.01	W86*						
		E202						
Compound 7	−8.56 ± 0.07	**Y72**	W86*	S293	F295	**Y341**		
		D74	**W286**	V294	F297			
Compound 8	−8.95 ± 0.13	**Y72**	W86*	**W286**	V294	F297		
		D74	**Y124**	S293	F295	**Y341**		
Compound 9	−9.46 ± 0.08	**Y72**	W86*	**W286**	V294	F297	**Y341**	
		D74	**Y124**	S293	F295	F338*		
Compound 10	−9.59 ± 0.07	**Y72**	W86*	**W286**	S293	F295	F297	F338*
		D74	**Y124**	L289	V294	R296	Y337	**Y341**
Compound 11	−9.79 ± 0.10	**Y72**	W86*	E202	S293	F295	Y337	**Y341**
		D74	**Y124**	**W286**	V294	F297	F338*	H447*

different orientations and interactions (Fig. 7C and 7D, and Table 2). We observed that the main conformation for theophylline was located close to the PAS site, making π-π interactions with W286 and Y341, π-alkyl interactions with Y72, L289, V294, F297, and F338, hydrophobic interactions with R296, and H-bonds with S293, F295, and R296 (Fig. 7C). The BBE observed for this conformation was about -5.3 Kcal/mol. Pyrrolidine only showed, instead, cation-π interaction with residues W86 and a salt bridge with E202, both residues from the CAS, with a BBE of about -4.8 Kcal/mol (Fig. 7D). All these observations are in line with our experimental results and suggest that theophylline can inhibit the AChE due to the number and type of interactions it could make in the PAS.

Finally, we extended our docking study to caffeine derivatives. We observed that the main cluster for each compound showed a similar location to that observed for donepezil. All compounds were placed in the CAS/PAS site with the pyrrolidine group orientated toward the CAS and the theophylline group interacting with residues in the PAS (Fig. 7E and 7F) with their BBE ranging from -8.56 and -9.79 Kcal/mol from compound **7** and **11**, respectively (Table 2). The pyrrolidine group showed the ability to interact with H447, which belongs to the ester subsite (crucial for the catalytic action of the enzyme), and make cation-π interaction with W86 and a salt bridge with D74 or E202 of the anionic subsite, similarly to that observed when pyrrolidine was docked alone (Fig. 7D). As it was expected, the theophylline group was placed mainly in the PAS and showed an increase in the number of residue interactions with the increase in the linker length (Table 2). Thus, while compound **7** showed π-π interactions with W286 and F297, π-alkyl interactions with Y72 and V294, and H-bonds with F295 and Y341, compound **11** showed π-π interactions with Y124, W286, F295, and Y341, π-alkyl interactions with Y72, W286, V294, and Y341, and H-bonds with Y124, F295, and Y341 (Fig. 7E, 7F and Table 2).

Thus, our docking results suggest that each compound can bind into the CAS/PAS site and interact with residues that were previously reported as key for AChE modulation (Quinn, 1987; Branduardi et al., 2005; Johnson and Moore, 2006). From the docking of each compound, we observed that the pyrrolidine group is important to stabilize and better orientate the theophylline group in the PAS. With the increase in the length of the linker chain, we observed an increase in the number of interactions between the theophylline group and key residues from the PAS, which suggests an improvement in the inhibition ability, which is in line with our experimental observations.

To extend our knowledge about the molecular interactions between each synthetic compound and the nAChR, we performed molecular docking studies. To this end, we modeled the extracellular domain of two adjacent subunits corresponding to the interfaces $\alpha1/\delta$ and $\alpha1/\varepsilon$ for the mouse muscle nAChR. Three loops from the α subunit (loops A-C) form the principal face and provide the aromatic residues Y93, W149, Y190, and 198, which stabilize the ammonium of the agonist (ACh or nicotine) by means of cation-π and H-bond interactions (Xiu et al., 2009). The subunit that forms the complementary face contributes with loops D, E and F, from which residues W55 and L119 have been reported to contribute to cation-π and/or H-bond interaction with the agonist, respectively (Karlin, 2002; Blum et al., 2010).

After binding of a full agonist, loop C closes to cover the binding pocket in a mechanism known as "capping" (Hansen et al., 2005). It was suggested that some partial agonists are unable to provoke a complete closure of loop C, which could be responsible for the partial channel response (Hibbs et al., 2009).

Since all compounds we tested in this work behave as partial agonists for the muscle nAChR, we evaluated their molecular interactions with two models, one with loop C in a closed conformation (named as "capped model"), and the other with loop C in a partially closed conformation (named as "partially capped model"). With both models, we then performed molecular dockings for each compound (Supplemental Figure 16).

As an initial control, we docked ACh in both interfaces ($\alpha1/\delta$ and $\alpha1/\varepsilon$) into the orthosteric binding site of the capped model (Fig. 8B). We observed that the most frequent conformation showed the lowest BBE (about -5.0 Kcal/mol). In this conformation, ACh adopted a similar orientation to that reported previously from the binding protein crystal structure (Olsen et al., 2014). ACh docked with its quaternary amine orientated to the lower part of the cleft, where it has the potential to form cation-π interactions with the abovementioned aromatic residues from the principal face, and cation-π with W55 and/or H-bond with L119, both from the complementary face (Fig. 8B).

We subsequently performed the same docking study for pyrrolidine and theophylline. We observed that pyrrolidine bound into the orthosteric binding site and the most frequent conformation (and with the lowest BBE of about -4.5 Kcal/mol) showed the ability to make interactions with residues from the principal face, but it lacked interactions with residues from the complementary face (Fig. 8C). In this conformation, the ammonium group of pyrrolidine, which is protonated at pH between 7.0 and 7.4, showed the potential to make a cation-π and H-bond interactions with W149, and a cation-π interaction with Y198 (Fig. 8C). All these results were similar to those reported previously for choline, a muscle nAChR partial agonist (Bruhova and Auerbach, 2017). The lack of interactions with residues from the complementary face could be responsible for the partial response observed for pyrrolidine since interactions with residues W55 and L119 have been reported as relevant for channel activation (Blum et al., 2010; Hernando et al., 2012). When we carried out the same analysis for theophylline, we observed that none of the conformations was able to dock into the orthosteric binding site. Therefore, we used the $\alpha1/\delta$ and $\alpha1/\varepsilon$ partially capped models. From these studies, we observed that the most frequent conformation, which was also the one with the lowest BBE (about -5.3 Kcal/mol), showed the potential to interact with residues from the binding site (Fig. 8D). In these models, theophylline showed the ability to form π-π staking with W149 and Y190, π-alkyl with W149 and C192, and H-bonds with W149 and Y198 from the principal face (Fig. 8D). This conformation also showed the ability to form π-alkyl with W55 and H-bond with L119, both residues from the complementary face (Fig. 8D).

We finally evaluated the ability of caffeine derivatives to bind into the orthosteric binding site of the nAChR. Based on the results we obtained with theophylline, we here carried out docking experiments with the partially capped

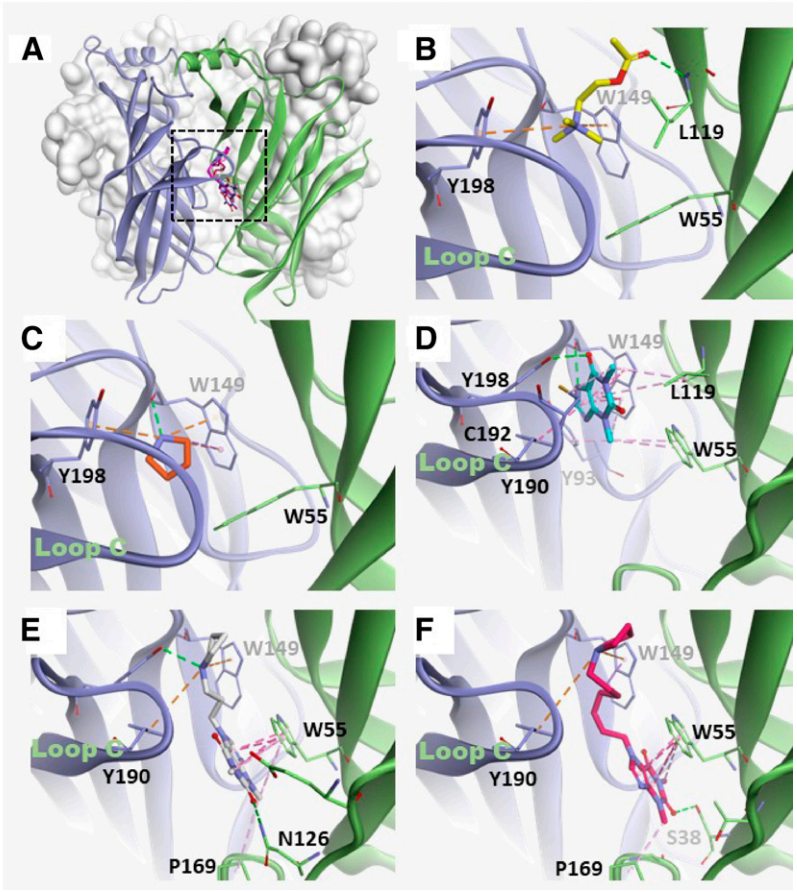

Fig. 8. Molecular docking of various compounds into the nicotinic acetylcholine receptor orthosteric binding site. A) Structure representation of the extracellular domain of the mouse nicotinic acetylcholine receptor. The $\alpha 1/\delta$ partially capped model interface is shown as ribbons, with $\alpha 1$ subunit in blue (principal face) and δ subunit in green (complementary face). The best conformation of compounds **7–11** is depicted in the orthosteric binding site. A detailed view of the region indicated with the black square (dashed lines) is shown for acetylcholine (B), pyrrolidine (C), theophylline (D), compound **7** (E), and compound **11** (F) with their corresponding interactions as dashed lines. Cation-π is shown in orange, π-alkyl in pink, π-π in purple and H-bond in green. For each ligand similar results were obtained with the corresponding $\alpha 1/\varepsilon$ models (not shown). For acetylcholine (B) and pyrrolidine (C) the subunit interface corresponds to the $\alpha 1/\delta$ capped model.

models. We observed that all compounds were able to bind into the binding pocket, where the most stable conformation showed similar frequency (about 20%) and BBE (about -7.5 Kcal/mol). In these conformations, each compound showed similar orientation, with the positive charge of the pyrrolidine group, making cation-π interactions with W149 and Y190, and H-bond with Y198, all residues from the principal face (Fig. 8E and 8F). The theophylline group was found to face the lower part of the pocket and showed the ability to make π-π stacking with W55, π-alkyl with W55 and P169, and H-bond with S38 or N126, all residues from the complementary face (Fig. 8E and 8F). All these results suggest that compounds **7–11** could make interactions with residues from the nAChR orthosteric binding pocket, which are critical for receptor response. However, this was only observed when the loop C was partially closed, which could be a plausible mechanism that explains why these compounds behave as partial agonists.

Discussion

AD is the principal cause of dementia among the elderly. Certain controversies remain about the causes and mechanisms of AD, and this is the reason why the development of new drugs for the treatment of this disease continues to be a great challenge (Dineley, 2007). The currently available medications, mainly inhibitors of the AChE, only ameliorate the symptoms in an early stage of the disease.

In a previous work, we postulated caffeine as an interesting molecule due to its potentiality to improve cholinergic transmission by a dual mechanism: inhibition of AChE and agonism of nAChRs (Fabiani et al., 2018). In this work, we obtained five caffeine derivatives by connecting theophylline and pyrrolidine through a methylene chain of different lengths.

We demonstrated that theophylline, like caffeine, inhibits the AChE, although it is less potent (Table 1). In contrast, pyrrolidine does not inhibit the AChE. We found that all derivatives inhibit the AChE with greater potency than caffeine, this effect being related to the length of the linker since compound **11** was the most potent, with an IC_{50} value two orders of magnitude higher than caffeine (Table 1). These results confirm that for AChE inhibition, the presence of a substituent at N-7 in the theophylline structure is essential.

To analyze the binding interactions of these compounds with the AChE, we performed molecular docking studies. We

worked with the structure of human AChE in complex with donepezil (PDB code 4EY7, Cheung et al., 2012). We first studied the location of theophylline and pyrrolidine and observed that while theophylline interacts mainly with residues from the PAS, pyrrolidine was docked in the CAS, without interaction with residues from the PAS, which could indicate that either the residues affected or the binding energy are not optimal to allow pyrrolidine to behave as an AChE inhibitor. The same results were found with respect to the synthetic analogs: the pyrrolidine group was docked in the CAS, while the structure corresponding to the theophylline was docked in the PAS. Thus, caffeine derivatives interact with residues similar to donepezil, corresponding to both sites, CAS and PAS, which could explain their ability to inhibit AChE. The length of the methylene chain of caffeine derivatives impacts their potency, probably by allowing a better location in both sites, which could explain why compound **11** showed the greatest AChE inhibition.

We then studied the effect of synthetic caffeine analogs on the nAChRs. Patch-clamp experiments showed that all compounds behaved as agonists of the muscle nAChR. Both chemical precursors behaved as partial agonists of the muscle receptor, showing an activation profile as isolated events. Caffeine analogs activated the muscle nAChR even at very low concentrations (picomolar range), which demonstrates that they behave as agonists with higher potency than caffeine (Fabiani et al., 2018). Based on our results, we confirmed that these compounds activate the muscle nAChR as isolated events without the ability to form clusters, even at high concentrations. Our results confirm that these compounds behave as potent partial agonists, similar to our observations from their precursors, theophylline and pyrrolidine, and that we reported previously for caffeine (Fabiani et al., 2018). To deepen our results, we obtained single-channel recordings from cells expressing the human α7 nAChR in the presence of compound **9**. This compound, in the absence of PNU, activates α7 receptor at concentrations 10-fold lower than those we reported for caffeine (Fabiani et al., 2018). Thus, we confirmed that the synthetic compounds behaved as agonists of both muscle and neuronal α7 nAChRs with higher potency than caffeine.

We then studied the muscle nAChR conformational state in the presence of the compounds. A first striking result was that theophylline showed no ability to stabilize the receptor in a desensitized conformation (Fig. 5), although, as stated above, it behaves as an agonist of the muscle nAChR (Fig. 2). This result reinforces the importance of the N-7 substituent because theophylline and caffeine have different effects on the conformational state of the nAChR. On the other hand, and contrary to expectations based on the importance of both cyclic groups of the nicotine for full nAChR activation (Graton et al., 2003; Blum et al., 2010), pyrrolidine not only activated the muscle nAChR (Fig. 2) but stabilized it in a desensitized conformational state (Fig. 5). Caffeine derivatives showed different effects on the nAChR conformational states depending on the length of the methylene chain linker (Fig. 6). While compounds **9** and **10** were able to desensitize the muscle nAChR, similarly to what was observed with pyrrolidine and previously reported for caffeine and carb (Fabiani et al., 2018), compounds **7**, **8,** and **11** behaved like theophylline, i.e., although by electrophysiological experiments we observed that they activated the muscle nAChR, CrV experiments confirmed that they did not stabilize the receptor in a desensitized conformation at all concentration ranges. It is probably that these compounds make different non-covalent interactions at the binding site which may result in diverse desensitized states, some more stable or deeper than others, and hence, in one case, the receptor stabilizes in a desensitized state, and in the other it either returns rapidly to a resting state (Reitstetter et al., 1999) or does not arrive to this state at all. In all cases, the addition of carb after incubation with compounds **7–11** confirmed that the compounds did not alter the response of nAChR to agonist, indicating that they do not exert a main inhibitory effect as described before for QX 314 (channel blocker) or α-bungarotoxin (competitive antagonist) (Fabiani et al., 2018).

To deepen our results, we performed molecular docking experiments. The orthosteric agonist binding sites are in the extracellular domain at the interface between two subunits. These sites are formed by six loops distributed on two faces: a principal face (α subunit), formed by loops A, B, and C and a complementary face formed by loops D, E, and F (non-α subunit). Following agonist binding, loop C closes to cover the binding site in a mechanism known as capping, that was suggested as crucial for channel gating (Hansen et al., 2005; Mukhtasimova et al., 2009). Different structures were solved in the absence or in the presence of ligands. They show that loop C is in an uncapped conformation in the absence of ligand or in the presence of antagonists (Hansen et al., 2005; Billen et al., 2012). When a partial agonist is bound, loop C adopts a partially capped conformation, which was suggested as responsible for the partial receptor response (Hibbs et al., 2009; Billen et al., 2012; Spurny et al., 2015).

We generated two homology models for each of the orthosteric binding sites for the mouse muscle nAChR, one model with loop C in a capped conformation and one with loop C in a partially capped conformation. Pyrrolidine mainly interacts with the capped model. The main conformation was placed toward the principal face of the binding pocket, and it did not show interactions with residues from the complementary face, similar to choline, a classic muscle nAChR partial agonist (Bruhova and Auerbach, 2017). The lack of interactions with residues from the complementary face could be responsible for the partial response observed for pyrrolidine. Theophylline could interact with the orthosteric binding site only in the partially capped model showing different interactions with residues from the principal and complementary face. Since at pH between 7.0 and 7.4, theophylline is mainly in the unprotonated form, it could not form cation-π interactions with residues from the binding site. Therefore, the partially capped conformation of the receptor and the lack of cation-π interactions between theophylline and residues from the binding site are plausible explanations for the partial response observed.

Similarly to theophylline, all compounds docked into the orthosteric binding site only when the loop C was partially closed. Unlike what we observed from docking studies with AChE, compounds **7–11** showed similar conformations, which suggests that the length of the linker was not a relevant characteristic for nAChR activation. The theophylline group was placed in the lower part of the binding pocket making interactions with residues from the complementary face. Therefore, in spite of their ability to make cation-π interactions with residues from the principal face, the partially

capped conformation and the type of interactions with residues from the complementary face seem to be possible mechanisms that explain the action as a partial agonist for the synthetized compounds.

In this work, we synthetized five novel hybrid-compounds, analogs of the caffeine, which can inhibit the AChE and activate both muscle and α7 nAChRs with higher potency than caffeine. Based on our results, caffeine analogs can be divided into two groups. Although all of them activate nAChRs, some of them conduct the receptor to a desensitized and agonist-refracting state, while others make the receptor to quickly return to a resting, agonist-responding state. The different effect depends on the length of the linker between theophylline and pyrrolidine. This result is a novel structure-activity relationship that emerges in distinct hybrid-analogs. The fact that such a small difference in the structure produces a different effect on nAChR activity while maintaining the AChE inhibitory effect offers novel and very interesting options in drug design, giving valuable tools to transform the search of new drugs from random screening to a detailed rational drug design. The choice of a particular group of compounds will depend on the desired specific biologic effect. For the treatment of AD, a pathology in which there is an important loss of cholinergic neurons, the fact that some analogs behave as potent agonists of the nAChRs avoiding receptor desensitization appears to be a promising therapy for the enhancing of cholinergic transmission. From the nAChR-non desensitizing group, compound **11** is the most interesting analog for further studies since it inhibits AChE with the highest potency and activates the nAChRs in the picomolar range without inducing receptor desensitization.

Authorship Contributions

Participated in research design: Fabiani, Biscussi, Murray, Corradi, Antollini.

Conducted experiments: Fabiani, Biscussi, Munafó.

Performed data analysis: Fabiani, Biscussi, Murray, Corradi and Antollini.

Wrote or contributed to the writing of the manuscript: Fabiani, Corradi, Antollini.

Acknowledgments

Esp. María de la Paz Guillon, Mg. Alicia B. Hernandez, Esp. Liliana A. García. Math Department, Universidad Nacional del Sur, Bahía Blanca, Argentina.

References

Akk G and Auerbach A (1999) Activation of muscle nicotinic acetylcholine receptor channels by nicotinic and muscarinic agonists. *Br J Pharmacol* **128**:1467–1476.

Alhowail A (2021) Molecular insights into the benefits of nicotine on memory and cognition (Review). *Mol Med Rep* **23**:398.

Barrantes FJ (1982) Oligomeric forms of the membrane-bound acetylcholine receptor disclosed upon extraction of the Mr 43,000 nonreceptor peptide. *J Cell Biol* **92**:60–68.

Barreto GE, Iarkov A, and Moran VE (2015) Beneficial effects of nicotine, cotinine and its metabolites as potential agents for Parkinson's disease. *Front Aging Neurosci* **6**:340.

Billen B, Spurny R, Brams M, van Elk R, Valera-Kummer S, Yakel JL, Voets T, Bertrand D, Smit AB, and Ulens C (2012) Molecular actions of smoking cessation drugs at $\alpha4\beta2$ nicotinic receptors defined in crystal structures of a homologous binding protein. *Proc Natl Acad Sci USA* **109**:9173–9178.

Biscussi B, Richmond V, Baier CJ, Mañez PA, and Murray AP (2020) Design and Microwave-Assisted Synthesis of Aza-Resveratrol Analogs with Potent Cholinesterase Inhibition. *CNS Neurol Disord Drug Targets* **19**:630–641.

Blum AP, Lester HA, and Dougherty DA (2010) Nicotinic pharmacophore: the pyridine N of nicotine and carbonyl of acetylcholine hydrogen bond across a subunit interface to a backbone NH. *Proc Natl Acad Sci USA* **107**:13206–13211.

Bouzat C, Lasala M, Nielsen BE, Corradi J, and Esandi MDC (2018) Molecular function of α7 nicotinic receptors as drug targets. J Physiol **596**:1847–1861.

Bouzat C, Barrantes F, and Sine S (2000) Nicotinic receptor fourth transmembrane domain: hydrogen bonding by conserved threonine contributes to channel gating kinetics. *J Gen Physiol* **115**:663–672.

Bouzat C, Bartos M, Corradi J, and Sine SM (2008) The interface between extracellular and transmembrane domains of homomeric Cys-loop receptors governs open-channel lifetime and rate of desensitization. *J Neurosci* **28**:7808–7819.

Bouzat C, Bren N, and Sine SM (1994) Structural basis of the different gating kinetics of fetal and adult acetylcholine receptors. *Neuron* **13**:1395–1402.

Branduardi D, Gervasio FL, Cavalli A, Recanatini M, and Parrinello M (2005) The role of the peripheral anionic site and cation-pi interactions in the ligand penetration of the human AChE gorge. *J Am Chem Soc* **127**:9147–9155.

Bruhova I and Auerbach A (2017) Molecular recognition at cholinergic synapses: acetylcholine versus choline. *J Physiol* **595**:1253–1261.

Carlson AB and Kraus GP (2020) Physiology, Cholinergic Receptors. Bookshelf ID: NBK526134.

Cheung J, Rudolph MJ, Burshteyn F, Cassidy MS, Gary EN, Love J, Franklin MC, and Height JJ (2012) Structures of human acetylcholinesterase in complex with pharmacologically important ligands. *J Med Chem* **55**:10282–10286.

Contestabile A (2011) The history of the cholinergic hypothesis. *Behav Brain Res* **221**:334–340.

Corradi J and Bouzat C (2016) Understanding the Bases of Function and Modulation of α7 Nicotinic Receptors: Implications for Drug Discovery. *Mol Pharmacol* **90**:288–299.

Corradi J, Spitzmaul G, De Rosa MJ, Costabel M, and Bouzat C (2007) Role of pairwise interactions between M1 and M2 domains of the nicotinic receptor in channel gating. *Biophys J* **92**:76–86.

Craig LA, Hong NS, and McDonald RJ (2011) Revisiting the cholinergic hypothesis in the development of Alzheimer's disease. *Neurosci Biobehav Rev* **35**:1397–1409.

daCosta CJ, Michel Sturgeon R, Hamouda AK, Blanton MP, and Baenziger JE (2011) Structural characterization and agonist binding to human $\alpha4\beta2$ nicotinic receptors. *Biochem Biophys Res Commun* **407**:456–460.

D'Andrea MR and Nagele RG (2006) Targeting the alpha 7 nicotinic acetylcholine receptor to reduce amyloid accumulation in Alzheimer's disease pyramidal neurons. *Curr Pharm Des* **12**:677–684.

Dani JA and Bertrand D (2007) Nicotinic acetylcholine receptors and nicotinic cholinergic mechanisms of the central nervous system. *Annu Rev Pharmacol Toxicol* **47**:699–729.

Davies P and Maloney AJ (1976) Selective loss of central cholinergic neurons in Alzheimer's disease. *Lancet* **2**:1403.

de Almeida JR, Figueiro M, Almeida WP, and de Paula da Silva CHT (2018) Discovery of novel dual acetylcholinesterase inhibitors with antifibrillogenic activity related to Alzheimer's disease. *Future Med Chem* **10**:1037–1053.

Dineley KT (2007) Beta-amyloid peptide–nicotinic acetylcholine receptor interaction: the two faces of health and disease. *Front Biosci* **12**:5030–5038.

Ellman GL, Courtney KD, Andres Jr V, and Feather-Stone RM (1961) A new and rapid colorimetric determination of acetylcholinesterase activity. *Biochem Pharmacol* **7**:88–95.

Fabiani C, Murray AP, Corradi J, and Antollini SS (2018) A novel pharmacological activity of caffeine in the cholinergic system. *Neuropharmacology* **135**:464–473.

Fu XW, Lindstrom J, and Spindel ER (2009) Nicotine activates and up-regulates nicotinic acetylcholine receptors in bronchial epithelial cells. *Am J Respir Cell Mol Biol* **41**:93–99.

Gandelman JA, Newhouse P, and Taylor WD (2018) Nicotine and networks: Potential for enhancement of mood and cognition in late-life depression. *Neurosci Biobehav Rev* **84**:289–298.

Graton J, Berthelot M, Gal JF, Laurence C, Lebreton J, Le Questel JY, Maria PC, and Robins R (2003) The nicotinic pharmacophore: thermodynamics of the hydrogen-bonding complexation of nicotine, nornicotine, and models. *J Org Chem* **68**:8208–8221.

Guo CN, Sun L, Liu GL, Zhao SJ, Liu WW, and Zhao YB (2015) Protective effect of nicotine on the cultured rat basal forebrain neurons damaged by β-Amyloid (Aβ)25-35 protein cytotoxicity. *Eur Rev Med Pharmacol Sci* **19**:2964–2972.

Hampel H, Mesulam MM, Cuello AC, Farlow MR, Giacobini E, Grossberg GT, Khachaturian AS, Vergallo A, Cavedo E, Snyder PJ, et al. (2018) The cholinergic system in the pathophysiology and treatment of Alzheimer's disease. *Brain* **141**:1917–1933.

Hansen SB, Sulzenbacher G, Huxford T, Marchot P, Taylor P, and Bourne Y (2005) Structures of Aplysia AChBP complexes with nicotinic agonists and antagonists reveal distinctive binding interfaces and conformations. *EMBO J* **24**:3635–3646.

Hernando G, Bergé I, Rayes D, and Bouzat C (2012) Contribution of subunits to Caenorhabditis elegans levamisole-sensitive nicotinic receptor function. *Mol Pharmacol* **82**:550–560.

Hibbs RE, Sulzenbacher G, Shi J, Talley TT, Conrod S, Kem WR, Taylor P, Marchot P, and Bourne Y (2009) Structural determinants for interaction of partial agonists with acetylcholine binding protein and neuronal alpha7 nicotinic acetylcholine receptor. *EMBO J* **28**:3040–3051.

Hurst RS, Hajós M, Raggenbass M, Wall TM, Higdon NR, Lawson JA, Rutherford-Root KL, Berkenpas MB, Hoffmann WE, Piotrowski DW, et al. (2005) A novel positive allosteric modulator of the alpha7 neuronal nicotinic acetylcholine receptor: in vitro and in vivo characterization. J Neurosci **25**:4396–4405.

Ijomone OM and Nwoha PU (2015) Nicotine inhibits hippocampal and striatal acetylcholinesterase activities, and demonstrates dual action on adult neuronal proliferation and maturation. *Pathophysiology* **22**:231–239.

Inestrosa NC, Sagal JP, and Colombres M (2005) Acetylcholinesterase interaction with Alzheimer amyloid beta. *Subcell Biochem* **38**:299–317.

Jarvik ME (1991) Beneficial effects of nicotine. *Br J Addict* **86**:571–575.

Johnson G and Moore SW (2006) The peripheral anionic site of acetylcholinesterase: structure, functions and potential role in rational drug design. *Curr Pharm Des* **12**:217–225.

Karlin A (2002) Emerging structure of the nicotinic acetylcholine receptors. *Nat Rev Neurosci* **3**:102–114.

Karlin A and Akabas MH (1995) Toward a structural basis for the function of nicotinic acetylcholine receptors and their cousins. *Neuron* **15**:1231–1244.
Lasala M, Fabiani C, Corradi J, Antollini S, and Bouzat C (2019) Molecular Modulation of Human α7 Nicotinic Receptor by Amyloid-β Peptides. *Front Cell Neurosci* **13**:37.
Laskowski RA, Moss DS, and Thornton JM (1993) Main-chain bond lengths and bond angles in protein structures. *J Mol Biol* **231**:1049–1067.
Le Novère N and Changeux JP (1995) Molecular evolution of the nicotinic acetylcholine receptor: an example of multigene family in excitable cells. J Mol Evol **40**:155–172.
Lurtz MM and Pedersen SE (1999) Aminotriarylmethane dyes are high-affinity noncompetitive antagonists of the nicotinic acetylcholine receptor. *Mol Pharmacol* **55**:159–167.
Ma KG and Qian YH (2019) Alpha 7 nicotinic acetylcholine receptor and its effects on Alzheimer's disease. *Neuropeptides* **73**:96–106.
Mackenbach JP, Damhuis RAM, and Been JV (2017) [The effects of smoking on health: growth of knowledge reveals even grimmer picture]. *Ned Tijdschr Geneeskd* **160**:D869.
Martorana A, Esposito Z, and Koch G (2010) Beyond the cholinergic hypothesis: do current drugs work in Alzheimer's disease? *CNS Neurosci Ther* **16**:235–245.
McKay BE, Placzek AN, and Dani JA (2007) Regulation of synaptic transmission and plasticity by neuronal nicotinic acetylcholine receptors. *Biochem Pharmacol* **74**:1120–1133.
Mishra A, Chaturvedi P, Datta S, Sinukumar S, Joshi P, and Garg A (2015) Harmful effects of nicotine. *Indian J Med Paediatr Oncol* **36**:24–31.
Morales-Perez CL, Noviello CM, and Hibbs RE (2016) X-ray structure of the human α4β2 nicotinic receptor. *Nature* **538**:411–415.
Morris GM, Huey R, Lindstrom W, Sanner MF, Belew RK, Goodsell DS, and Olson AJ (2009) AutoDock4 and AutoDockTools4: Automated docking with selective receptor flexibility. *J Comput Chem* **30**:2785–2791.
Mukhtasimova N, Lee WY, Wang HL, and Sine SM (2009) Detection and trapping of intermediate states priming nicotinic receptor channel opening. *Nature* **459**:451–454.
Olsen JA, Balle T, Gajhede M, Ahring PK, and Kastrup JS (2014) Molecular recognition of the neurotransmitter acetylcholine by an acetylcholine binding protein reveals determinants of binding to nicotinic acetylcholine receptors. *PLoS One* **9**:e91232.
Paterson D and Nordberg A (2000) Neuronal nicotinic receptors in the human brain. *Prog Neurobiol* **61**:75–111.
Perry EK, Tomlinson BE, Blessed G, Perry RH, Cross AJ, and Crow TT (1981) Noradrenergic and cholinergic systems in senile dementia of Alzheimer type. *Lancet* **2**:149.
Pohanka M (2012) Alpha7 nicotinic acetylcholine receptor is a target in pharmacology and toxicology. *Int J Mol Sci* **13**:2219–2238.
Qin F, Auerbach A, and Sachs F (1996) Estimating single-channel kinetic parameters from idealized patch-clamp data containing missed events. *Biophys J* **70**:264–280.
Quinn DM (1987) Acetylcholinesterase: enzyme structure, reaction dynamics, and virtual transition states. *Chem Rev* **87**:955–979.
Reitstetter R, Lukas RJ, and Gruener R (1999) Dependence of nicotinic acetylcholine receptor recovery from desensitization on the duration of agonist exposure. *J Pharmacol Exp Ther* **289**:656–660.
Rusted JM, Trawley S, Heath J, Kettle G, and Walker H (2005) Nicotine improves memory for delayed intentions. *Psychopharmacology (Berl)* **182**:355–365.
Sali A (1995) Comparative protein modeling by satisfaction of spatial restraints. *Mol Med Today* **1**:270–277.
Selkoe D, Mandelkow E, and Holtzman D (2012) Deciphering Alzheimer disease. *Cold Spring Harb Perspect Med* **2**:a011460.
Shen MY and Sali A (2006) Statistical potential for assessment and prediction of protein structures. *Protein Sci* **15**:2507–2524.
Singh M, Kaur M, Kukreja H, Chugh R, Silakari O, and Singh D (2013) Acetylcholinesterase inhibitors as Alzheimer therapy: from nerve toxins to neuroprotection. *Eur J Med Chem* **70**:165–188.
Spurny R, Debaveye S, Farinha A, Veys K, Vos AM, Gossas T, Atack J, Bertrand S, Bertrand D, Danielson UH, et al. (2015) Molecular blueprint of allosteric binding sites in a homologue of the agonist-binding domain of the α7 nicotinic acetylcholine receptor. *Proc Natl Acad Sci USA* **112**:E2543–E2552.
Srivareerat M, Tran TT, Alzoubi KH, and Alkadhi KA (2009) Chronic psychosocial stress exacerbates impairment of cognition and long-term potentiation in beta-amyloid rat model of Alzheimer's disease. *Biol Psychiatry* **65**:918–926.
Whitehouse PJ and Au KS (1986) Cholinergic receptors in aging and Alzheimer's disease. *Prog Neuropsychopharmacol Biol Psychiatry* **10**:665–676.
Xiu X, Puskar NL, Shanata JA, Lester HA, and Dougherty DA (2009) Nicotine binding to brain receptors requires a strong cation-pi interaction. *Nature* **458**:534–537.

Address correspondence to: Silvia Susana Antollini, Instituto de Investigaciones Bioquímicas de Bahía Blanca, Departamento de Biología, Bioquímica y Farmacia, Universidad Nacional del Sur y Consejo Nacional de Investigaciones Científicas y Técnicas, Camino La Carrindanga km 7, Bahia Blanca, 8000, Argentina. E-mail: silviant@criba.edu.ar

SUPPLEMENTARY INFORMATION

NEW SYNTHETIC CAFFEINE ANALOGS AS MODULATORS OF THE CHOLINERGIC SYSTEM

Camila Fabiani[1], Brunella Biscussi[2], Juan P. Munafó[1], Ana P. Murray[2]*, Jeremías Corradi[1]*, Silvia S. Antollini[1]*

[1]Instituto de Investigaciones Bioquímicas de Bahía Blanca, Departamento de Biología, Bioquímica y Farmacia, Universidad Nacional del Sur y Consejo Nacional de Investigaciones Científicas y Técnicas, Camino La Carrindanga km 7, 8000 Bahía Blanca, Argentina
[2]Instituto de Química del Sur, Departamento de Química, Universidad Nacional del Sur y Consejo Nacional de Investigaciones Científicas y Técnicas, Av. Alem 1253, 8000 Bahía Blanca, Argentina
*Corresponding authors: silviant@criba.edu.ar; jcorradi@criba.edu.ar; apmurray@uns.edu.ar

Supplementary Figure S1

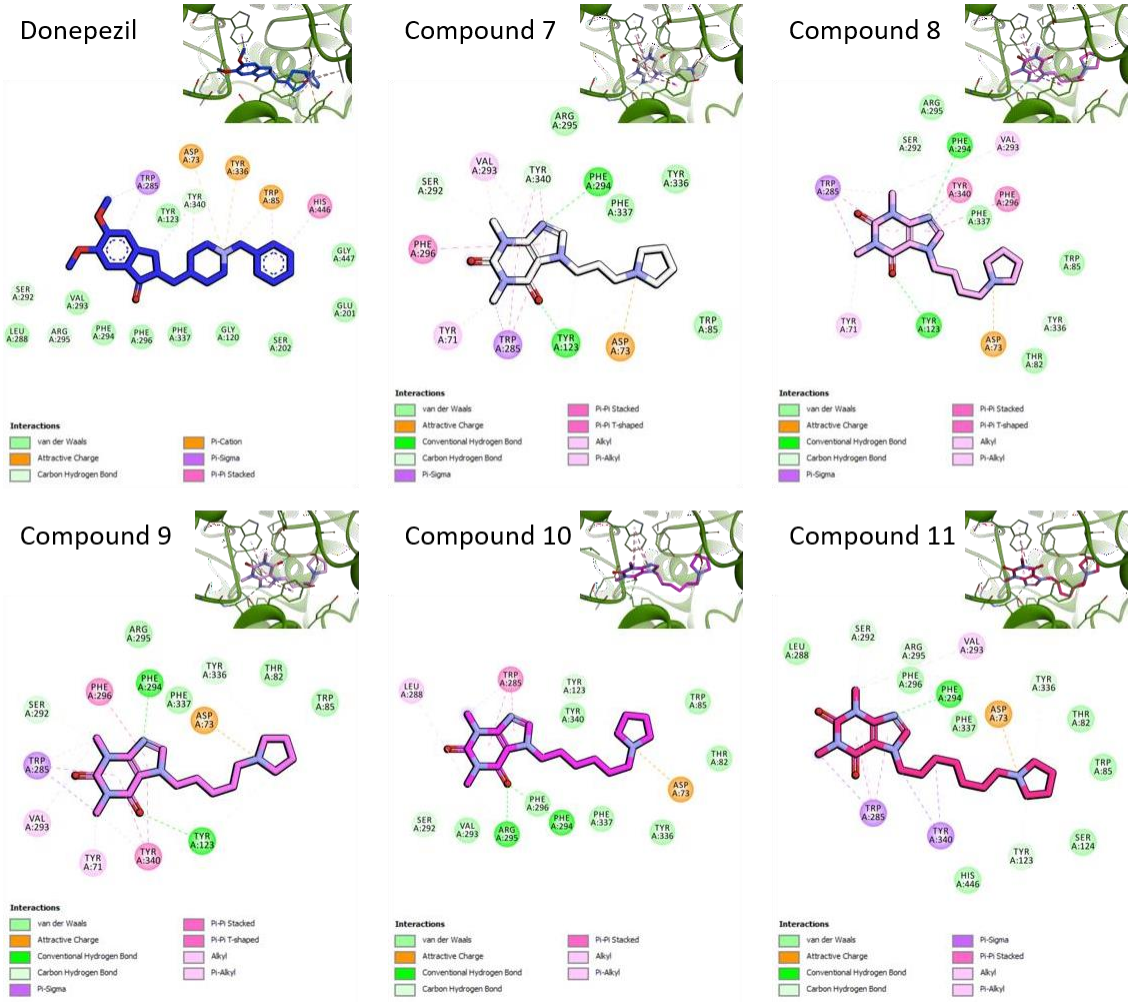

Figure S1: Ligand-receptor interaction for the best binding conformation of each ligand in the human AChE structure (PDB code 4EY7). 2D plots for ligand-receptor interactions are shown with the interacting residues within 4 Å of the docked compounds shown as spheres. *Inset*) 3D conformation of the corresponding ligand-receptor conformation, with AChE as green ribbons and ligands as sticks. For both representations the ligand-receptor interactions are shown in different colors.

Supplementary Figure S2

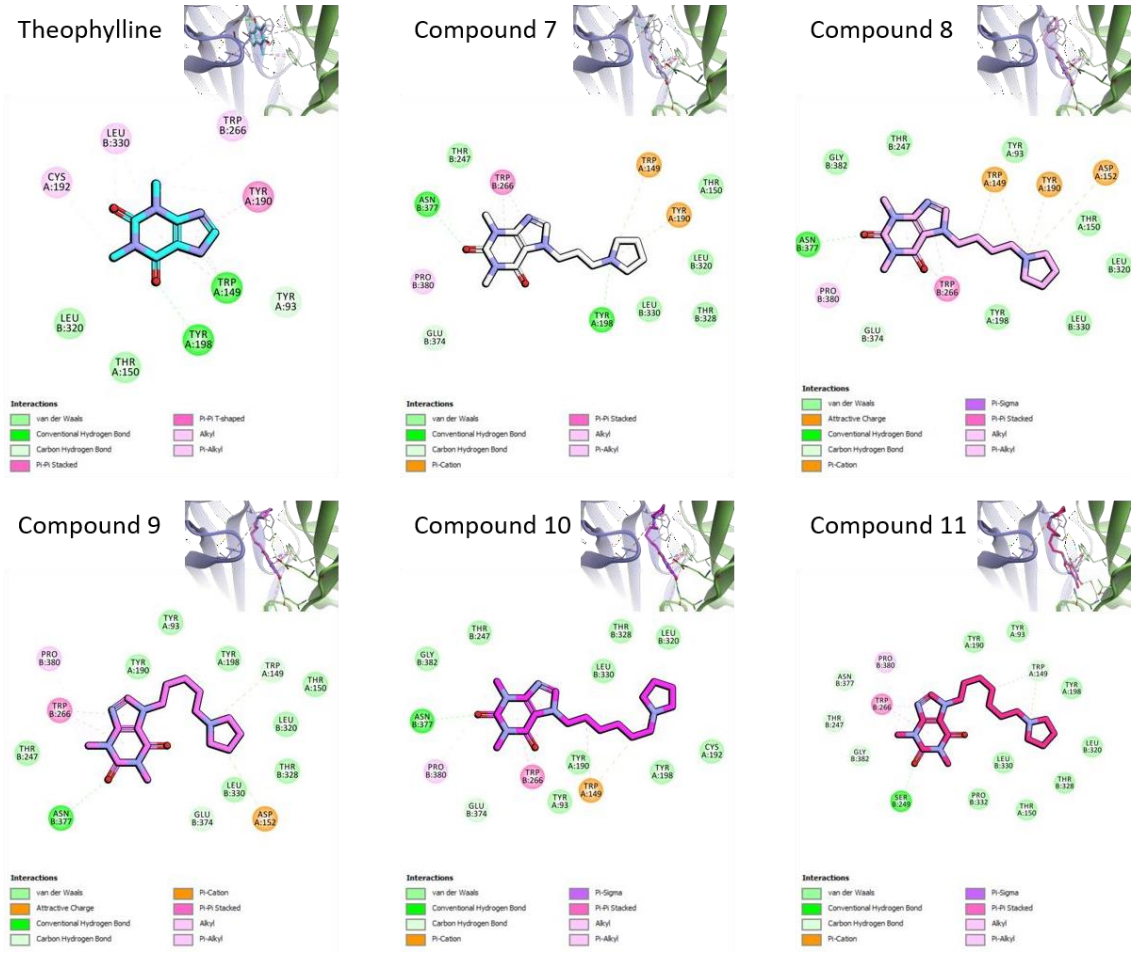

Figure S2: Ligand-receptor interaction for the best binding conformation of each ligand in the mouse α1/δ interface of the nAChR (partially capped model). 2D plots for ligand-receptor interactions are shown with the interacting residues within 4 Å of the docked compounds shown as spheres. Inset) 3D conformation of the corresponding ligand-receptor conformation, with nAChR as ribbons (α1 subunit in blue and δ subunit in green) and ligands as sticks. For both representations the ligand-receptor interactions are shown in different colors.

Supplementary Figure S3. ^{1}H NMR (300 MHz) and ^{13}C NMR (75 MHz) spectra in $CDCl_3$ of **2**

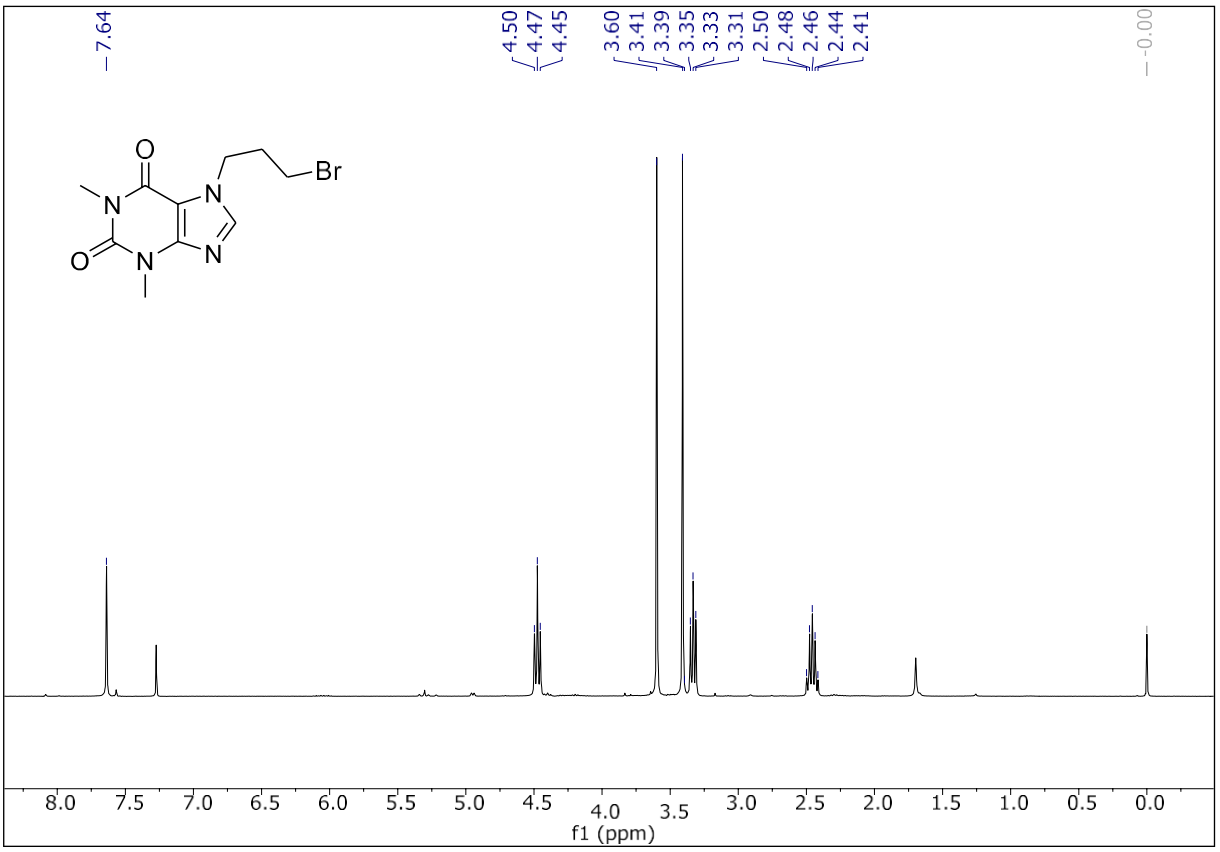

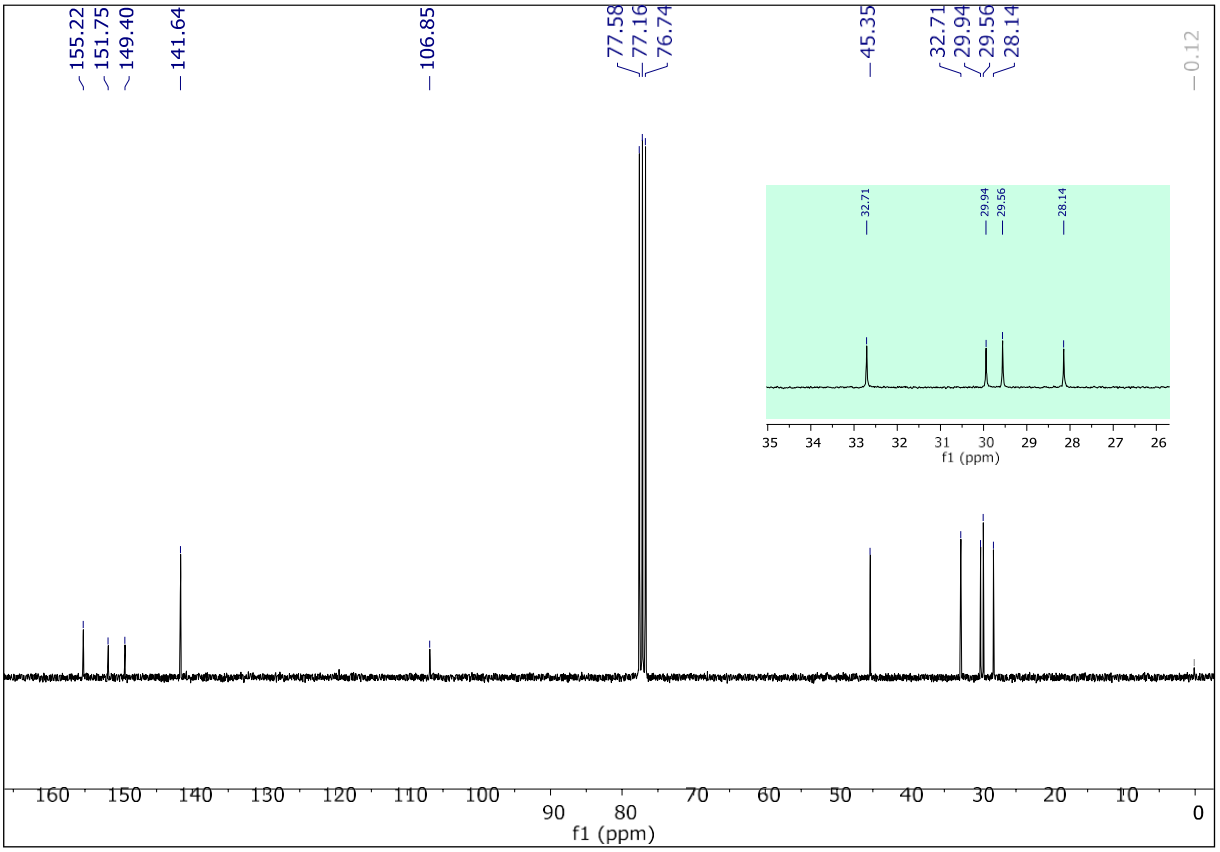

Supplementary Figure S4. 1H NMR (300 MHz) and 13C NMR (75 MHz) spectra in CDCl3 of **3**

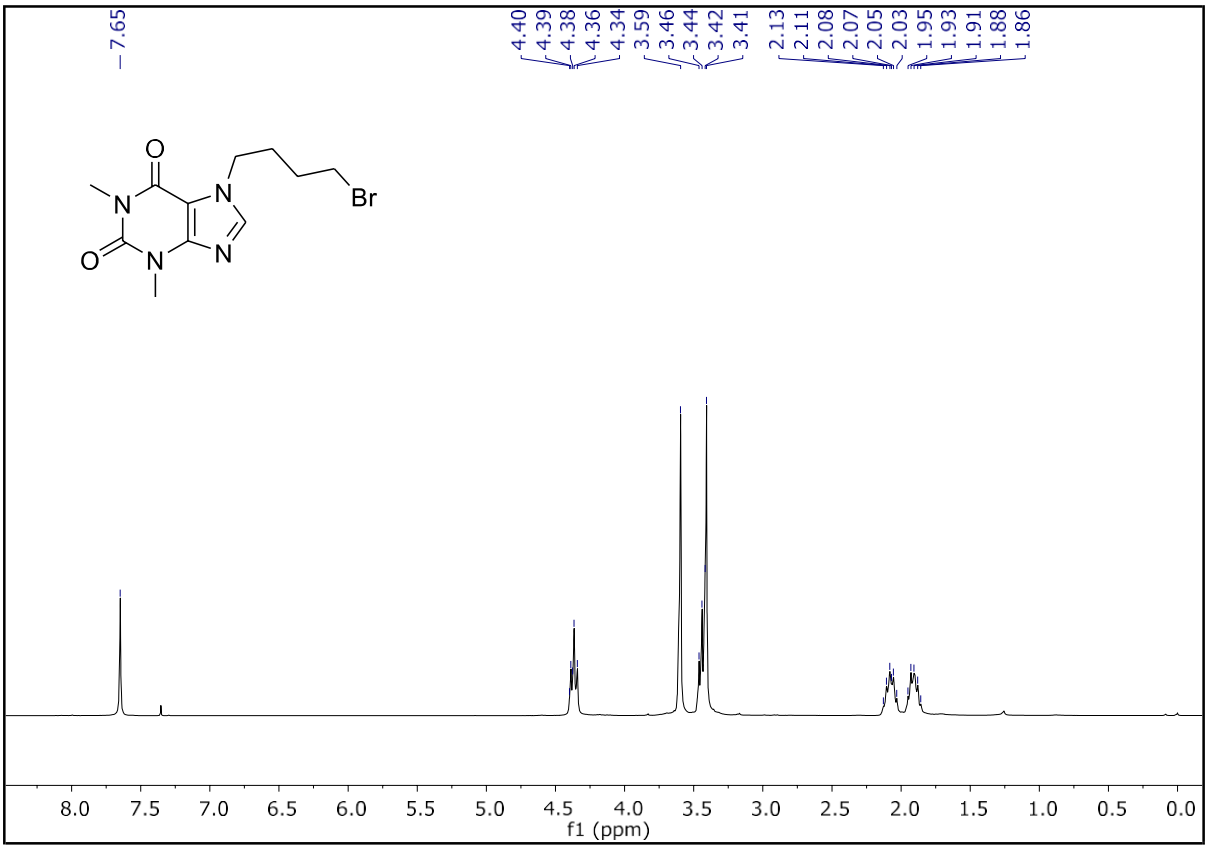

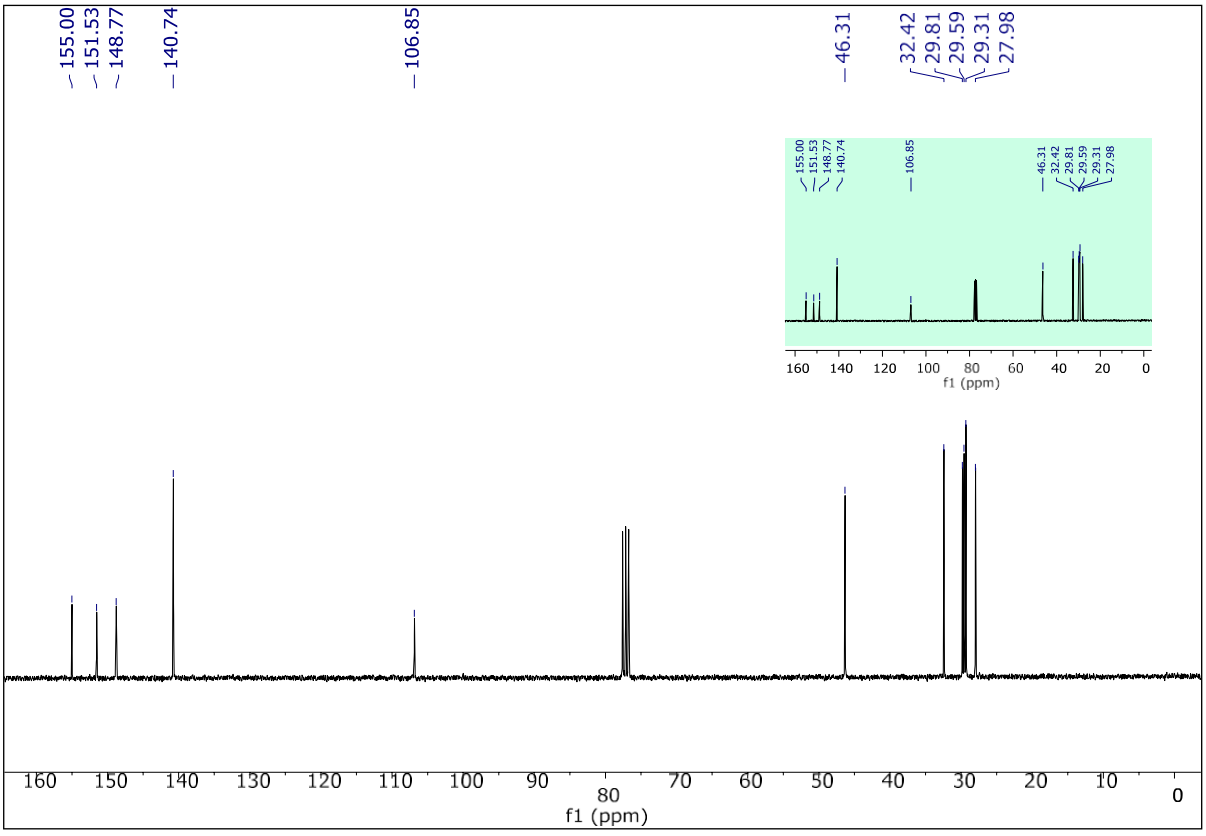

Supplementary Figure S5. ^{1}H NMR (300 MHz) and ^{13}C NMR (75 MHz) spectra in $CDCl_3$ of **4**

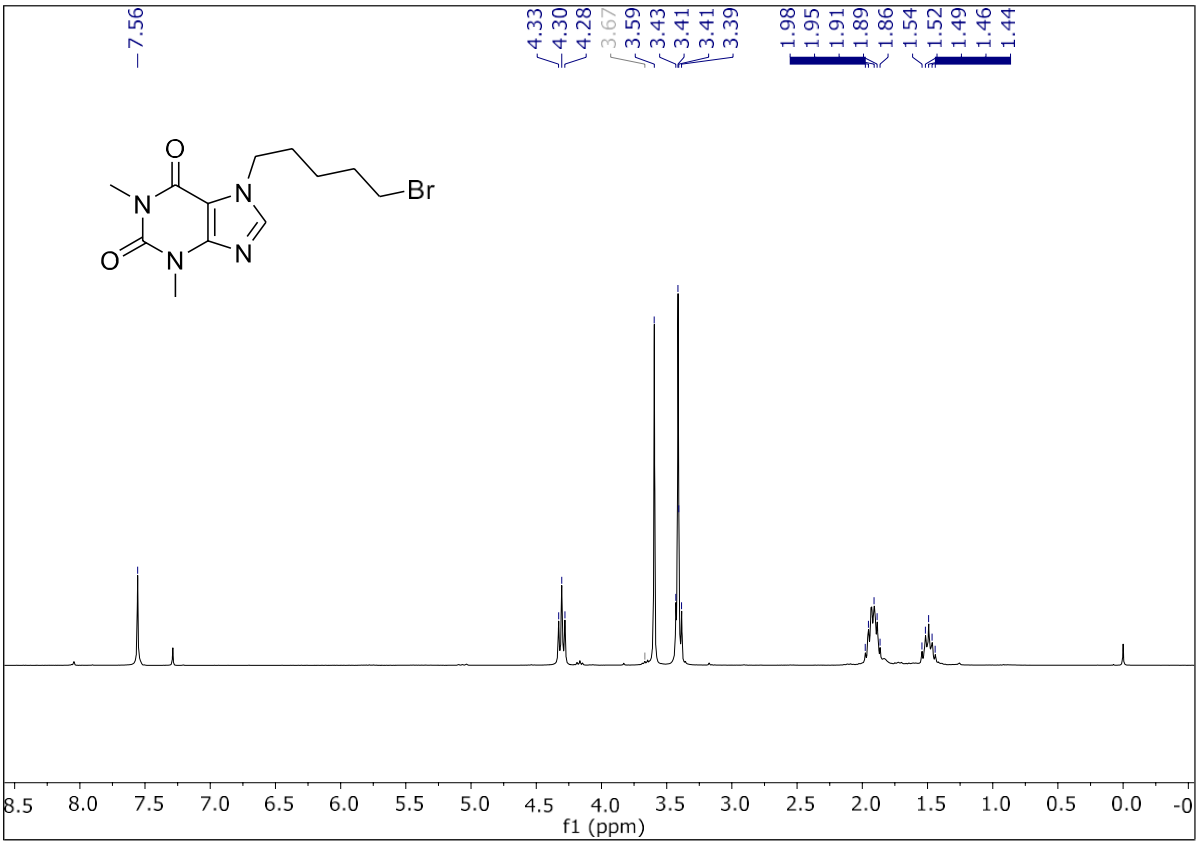

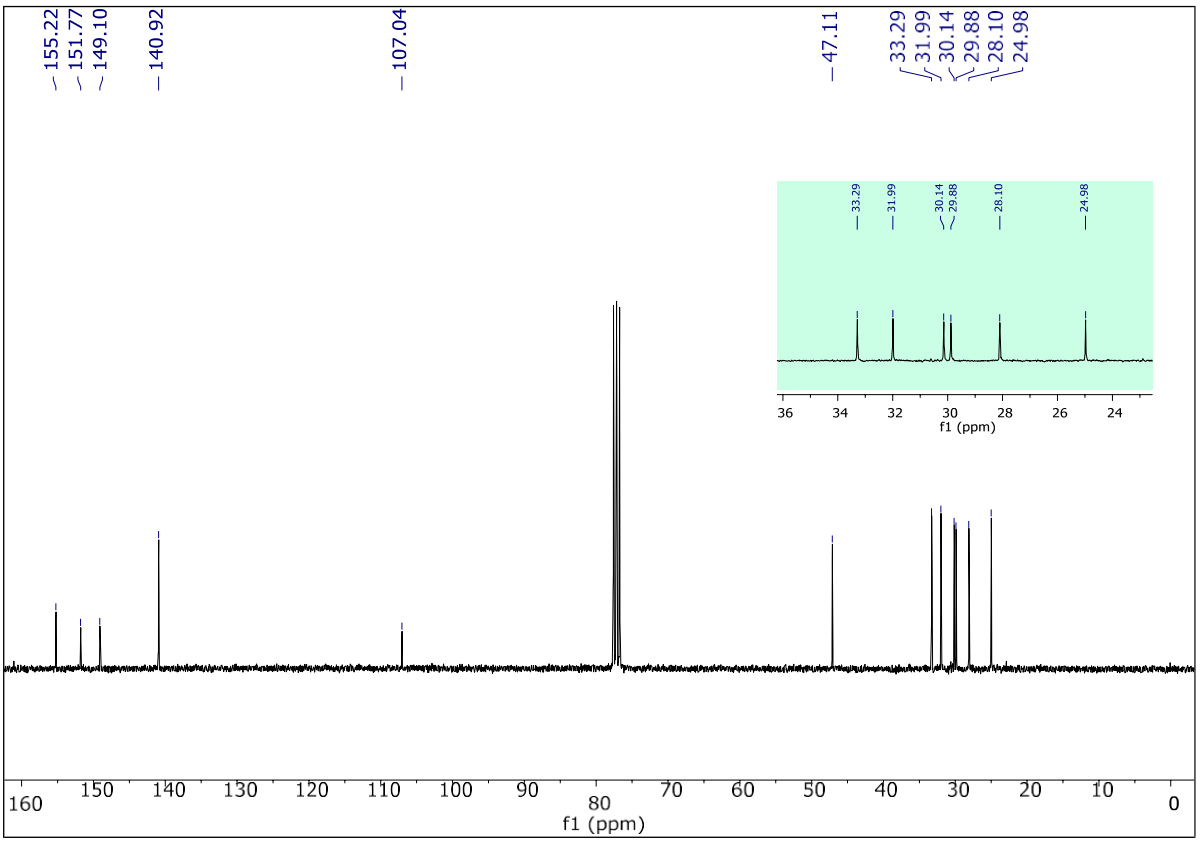

Supplementary Figure S6. HSQC and DEPT spectra in $CDCl_3$ of **4**

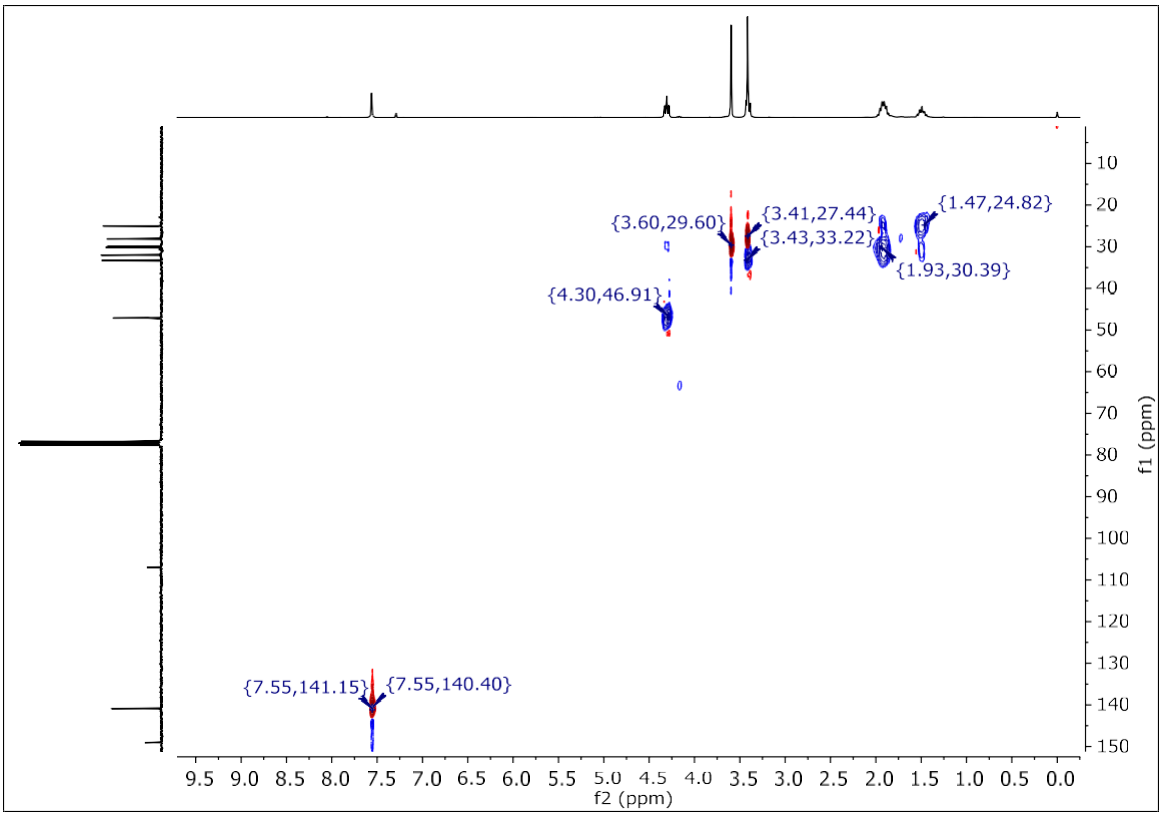

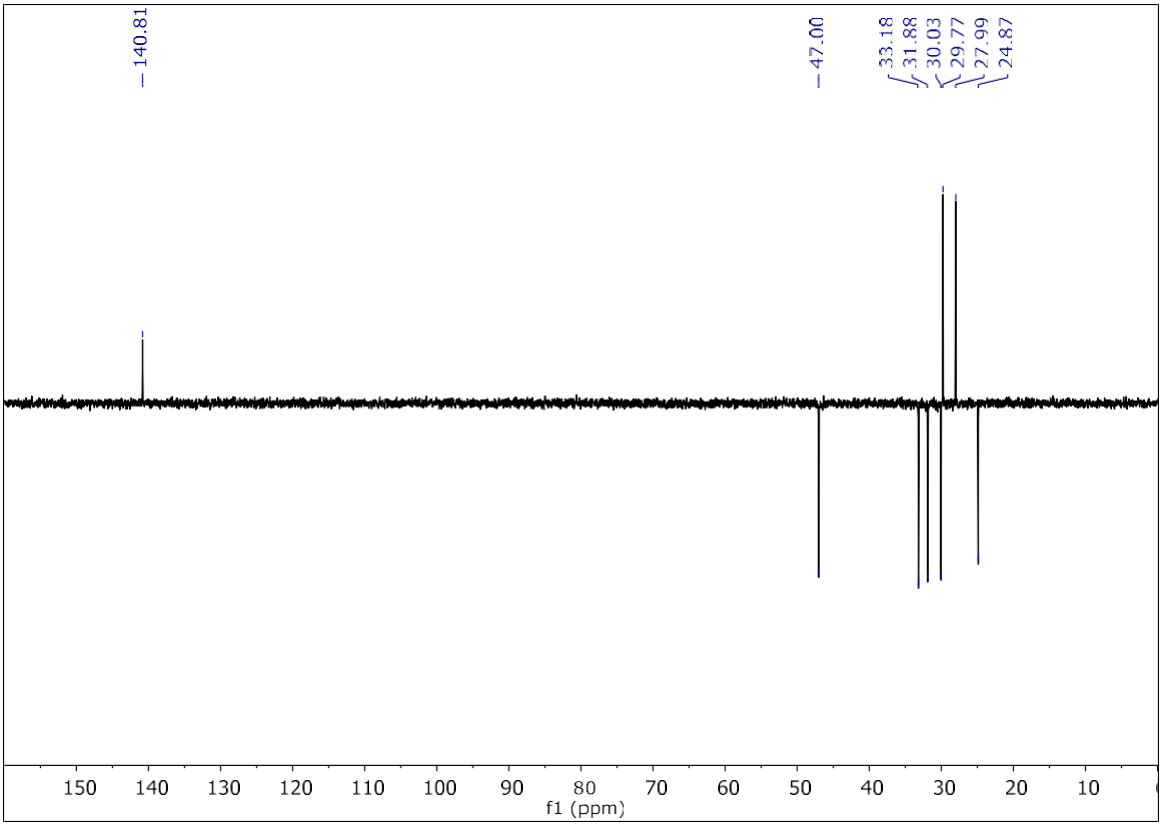

Supplementary Figure S7. ^{1}H NMR (300 MHz) and ^{13}C NMR (75 MHz) spectra in $CDCl_3$ of **5**

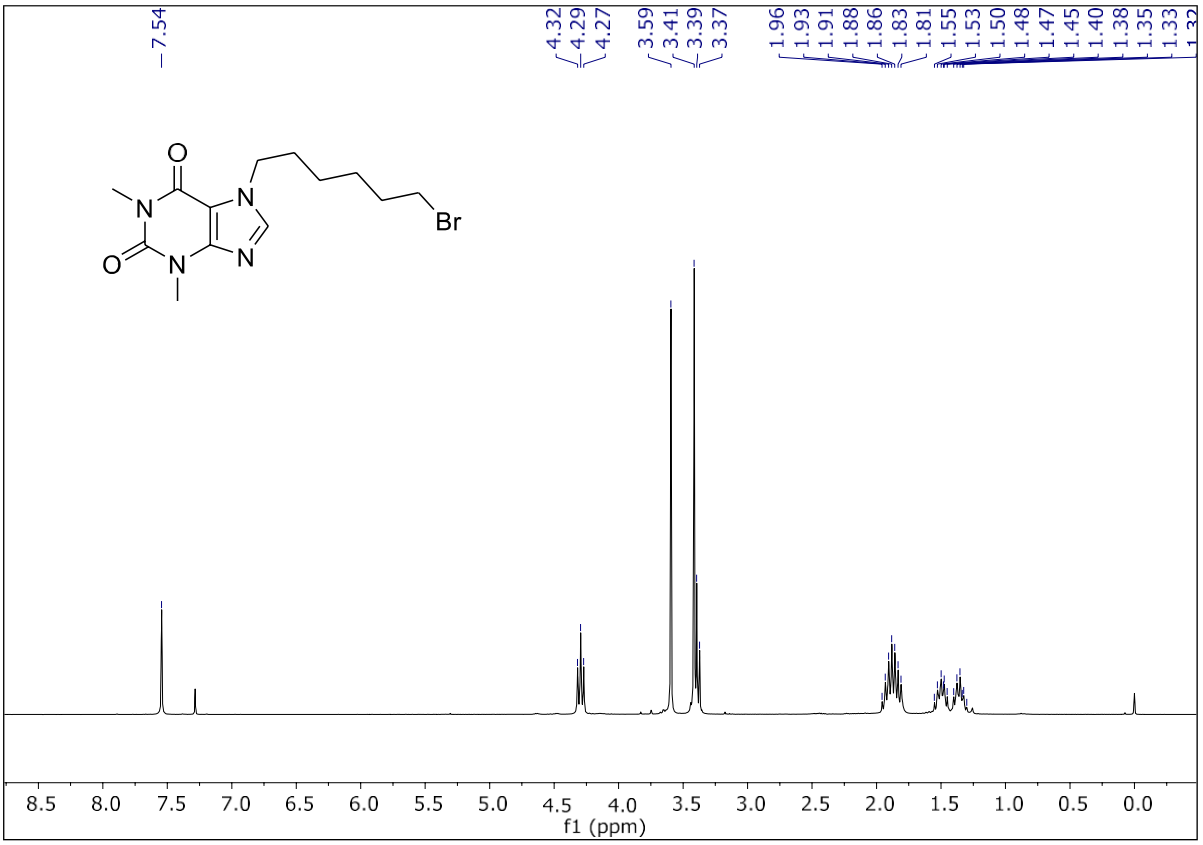

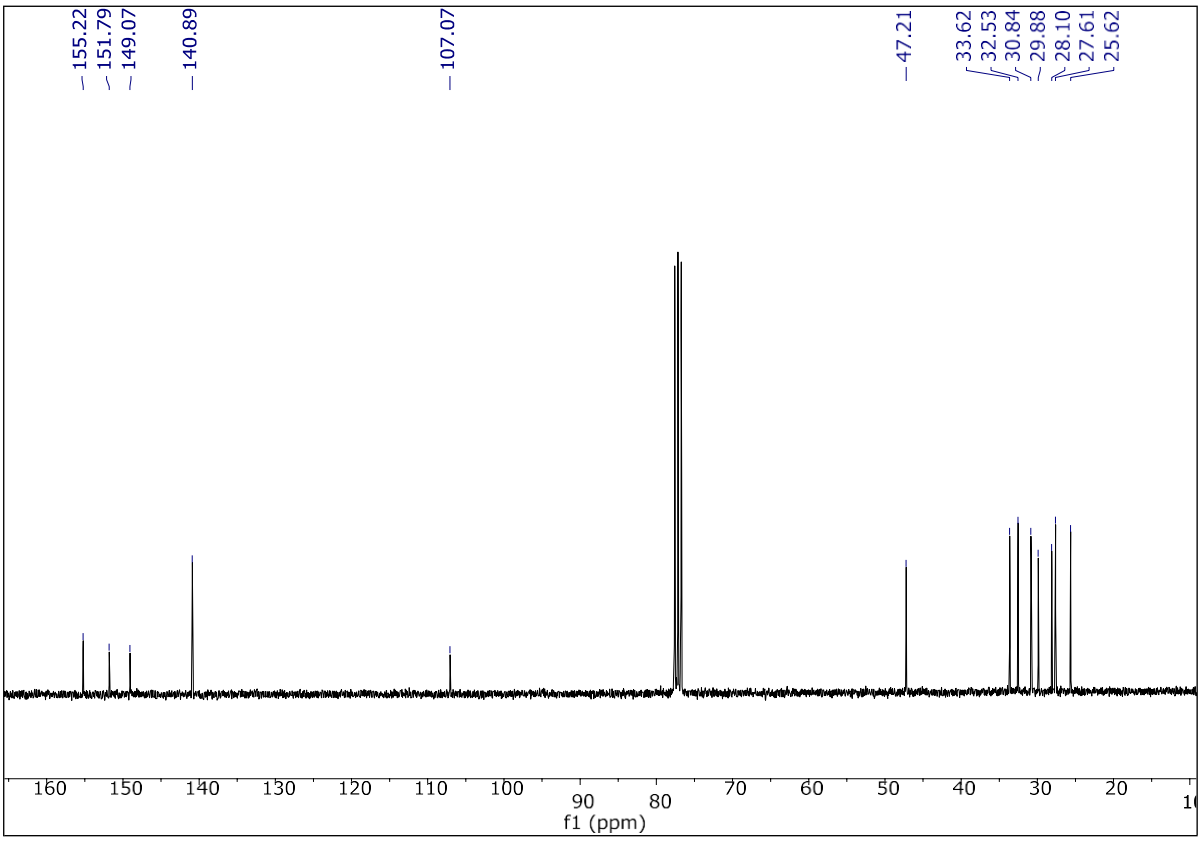

Supplementary Figure S8. ^{1}H NMR (300 MHz) and ^{13}C NMR (75 MHz) spectra in $CDCl_3$ of **7**

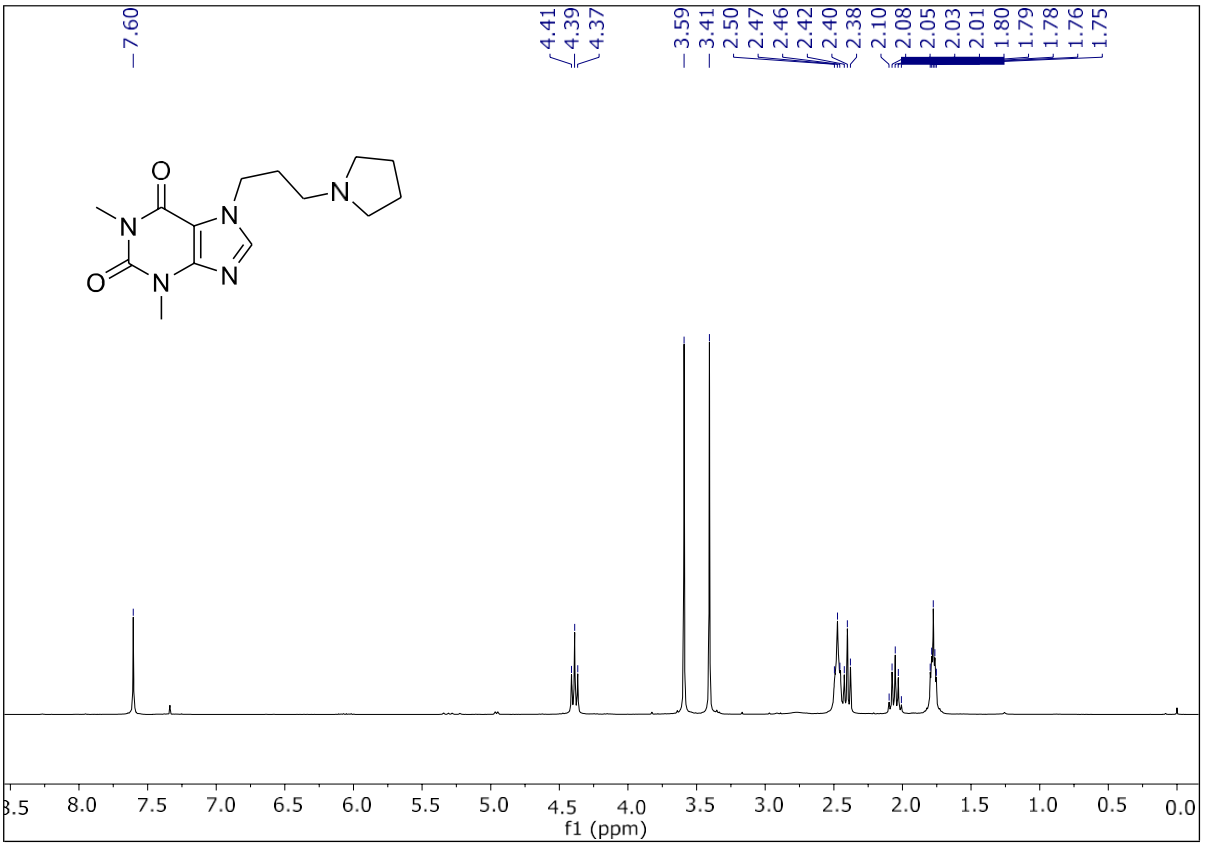

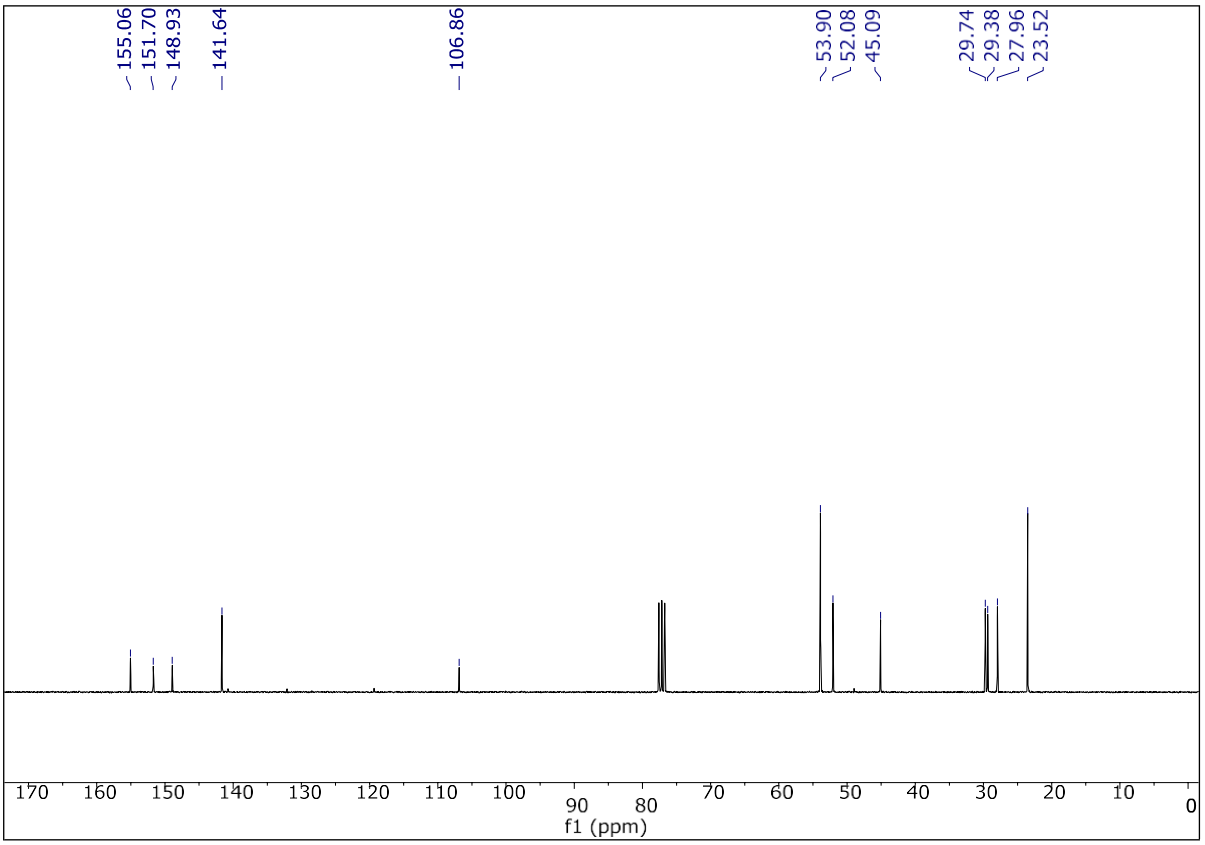

Supplementary Figure S9. ^{1}H NMR (300 MHz) and ^{13}C NMR (75 MHz) spectra in $CDCl_3$ of **8**

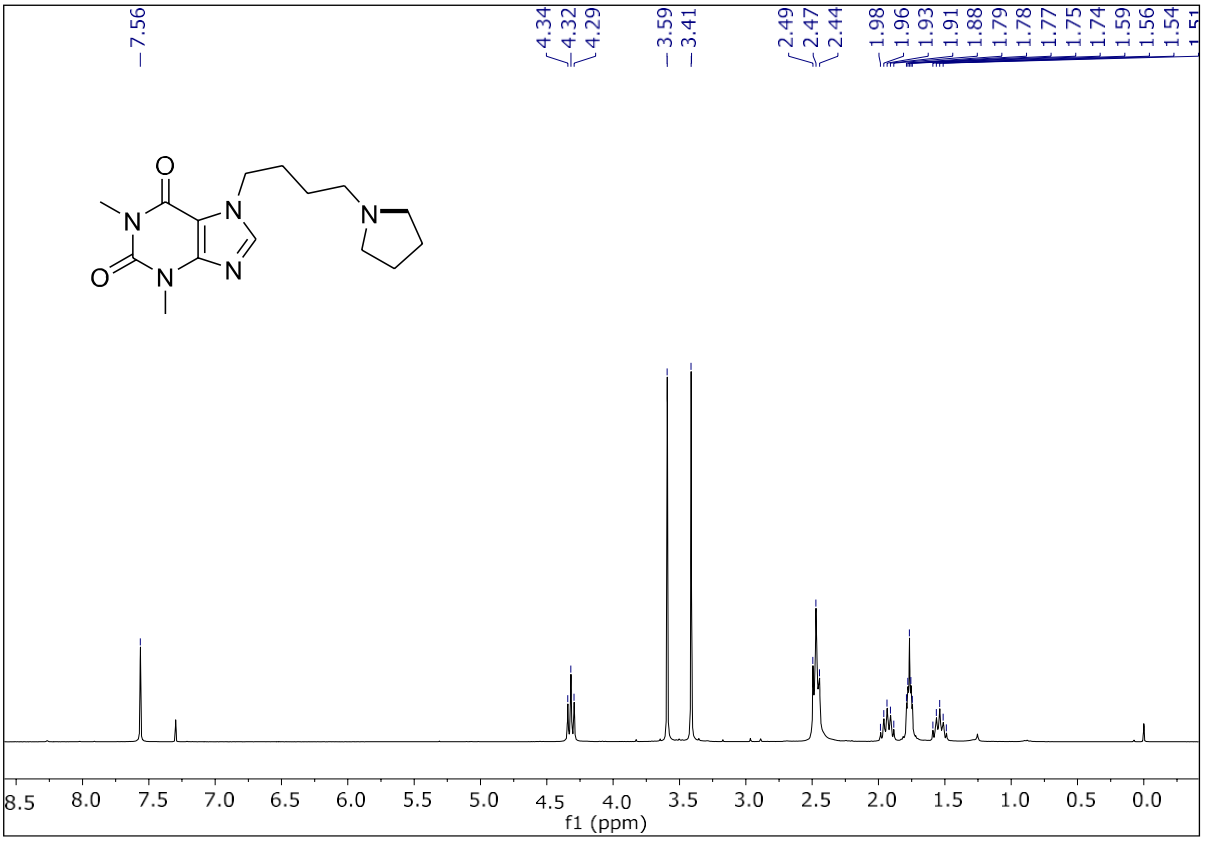

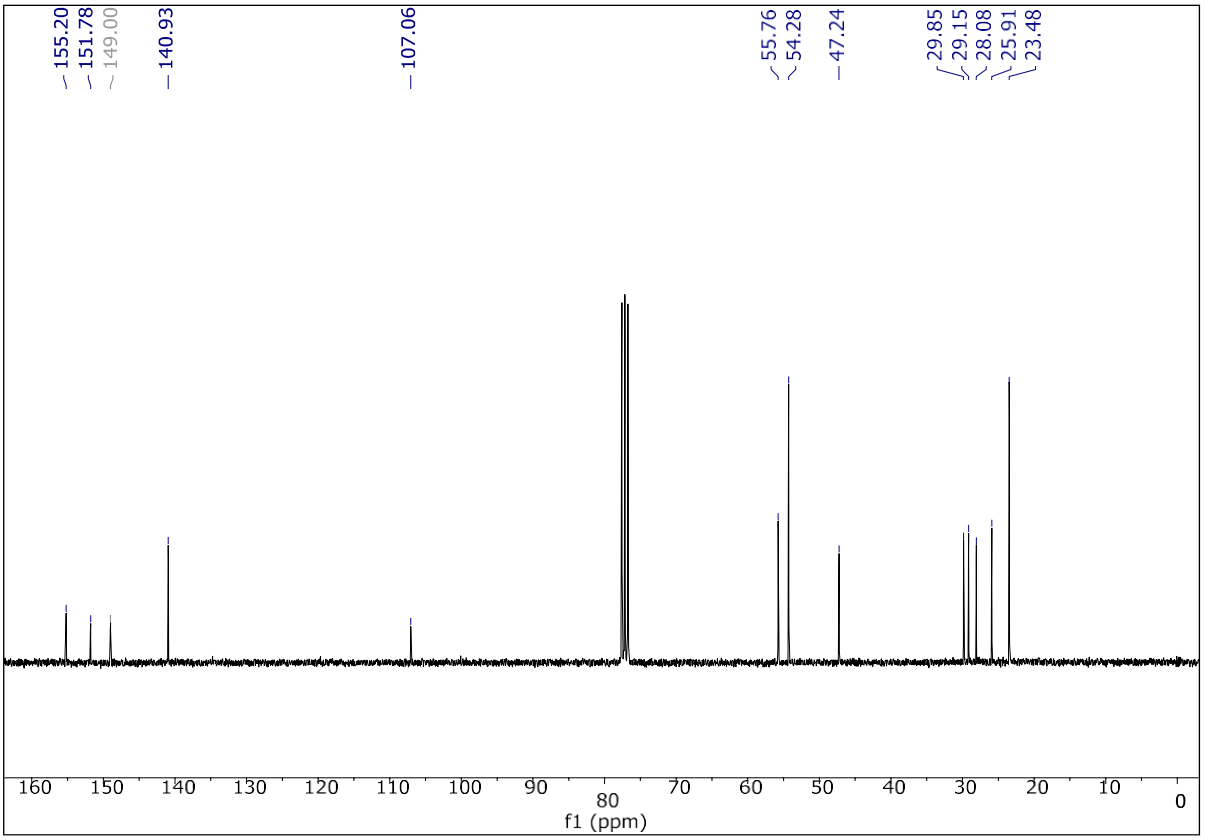

Supplementary Figure S10. HSQC and DEPT spectra in $CDCl_3$ of **8**

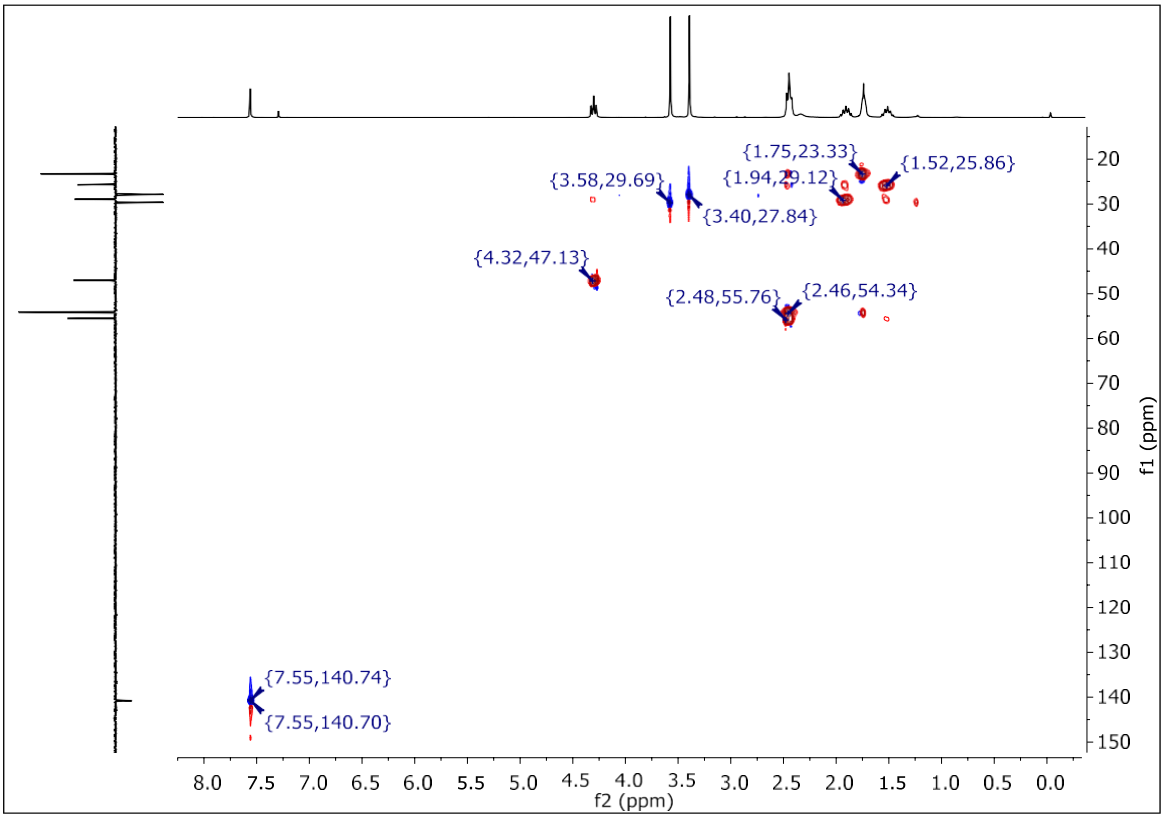

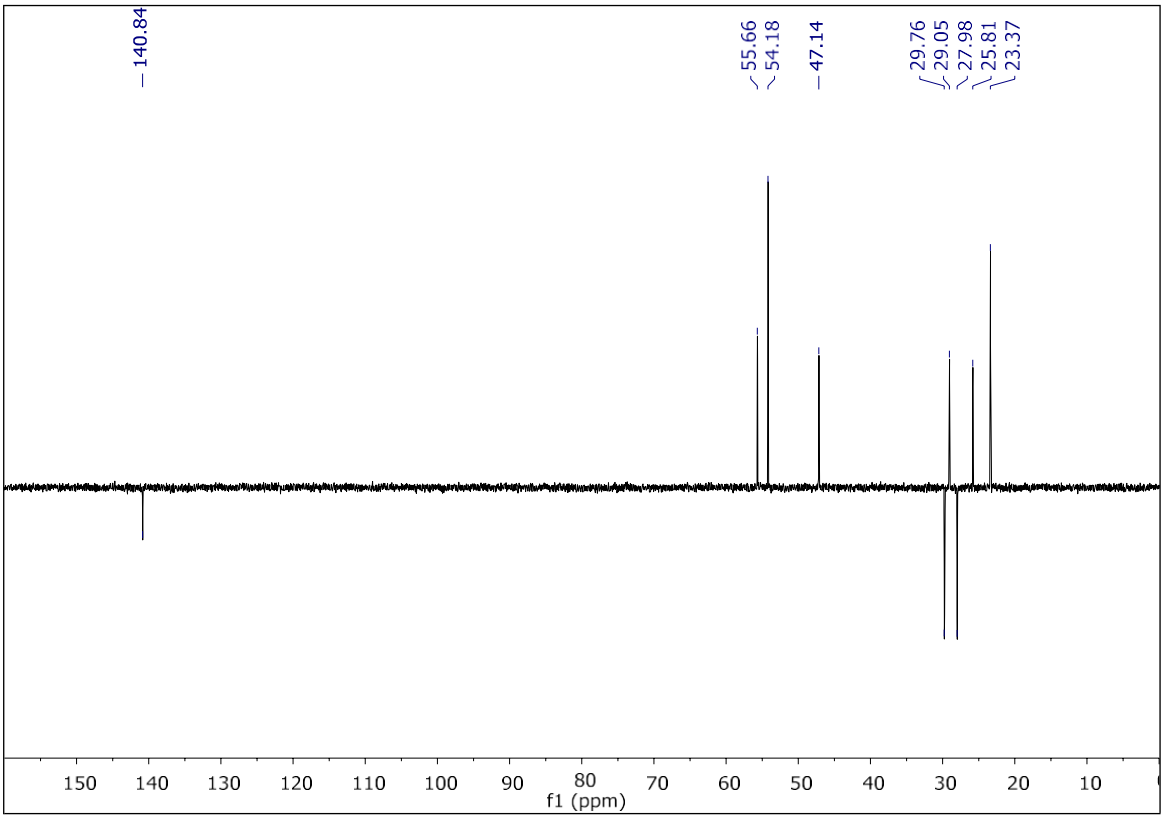

Supplementary Figure S11. ^{1}H NMR (300 MHz) and ^{13}C NMR (75 MHz) spectra in $CDCl_3$ of **9**

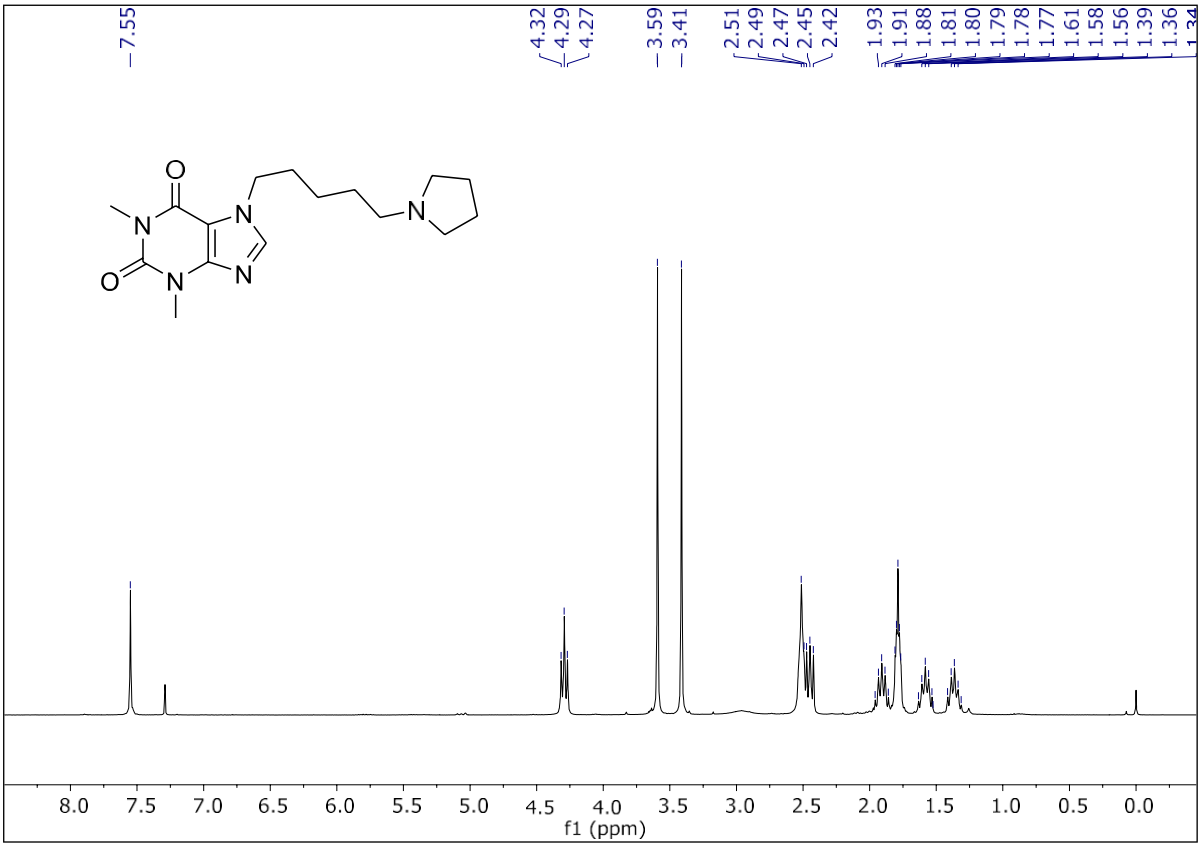

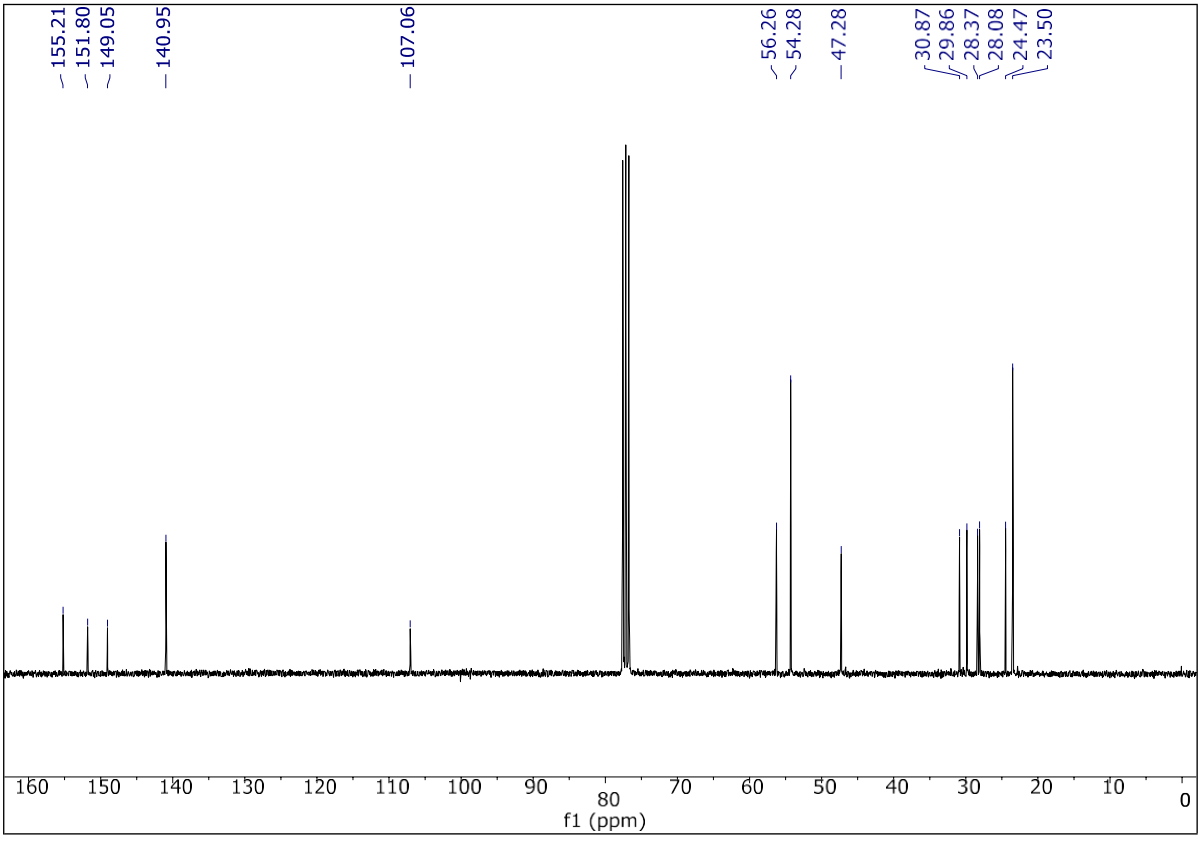

Supplementary Figure S12. HSQC and DEPT spectra in $CDCl_3$ of **9**

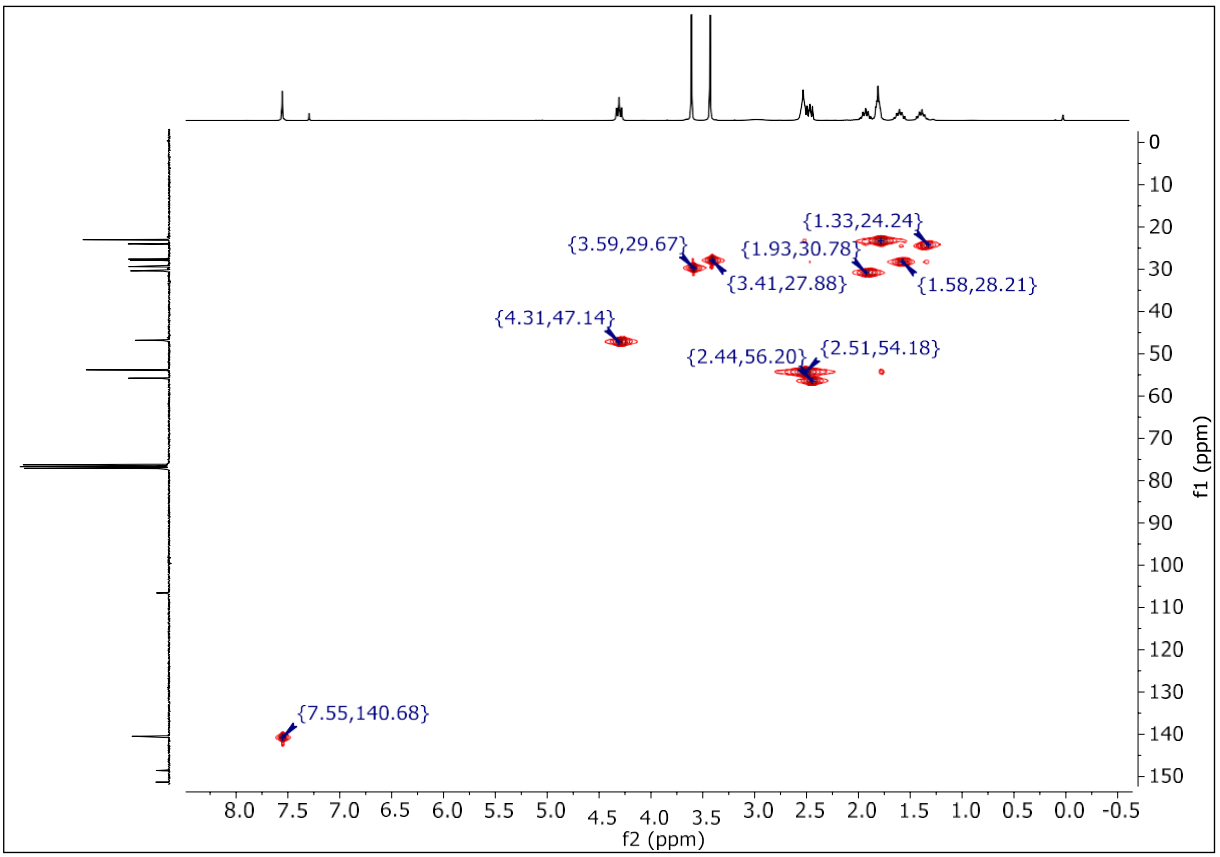

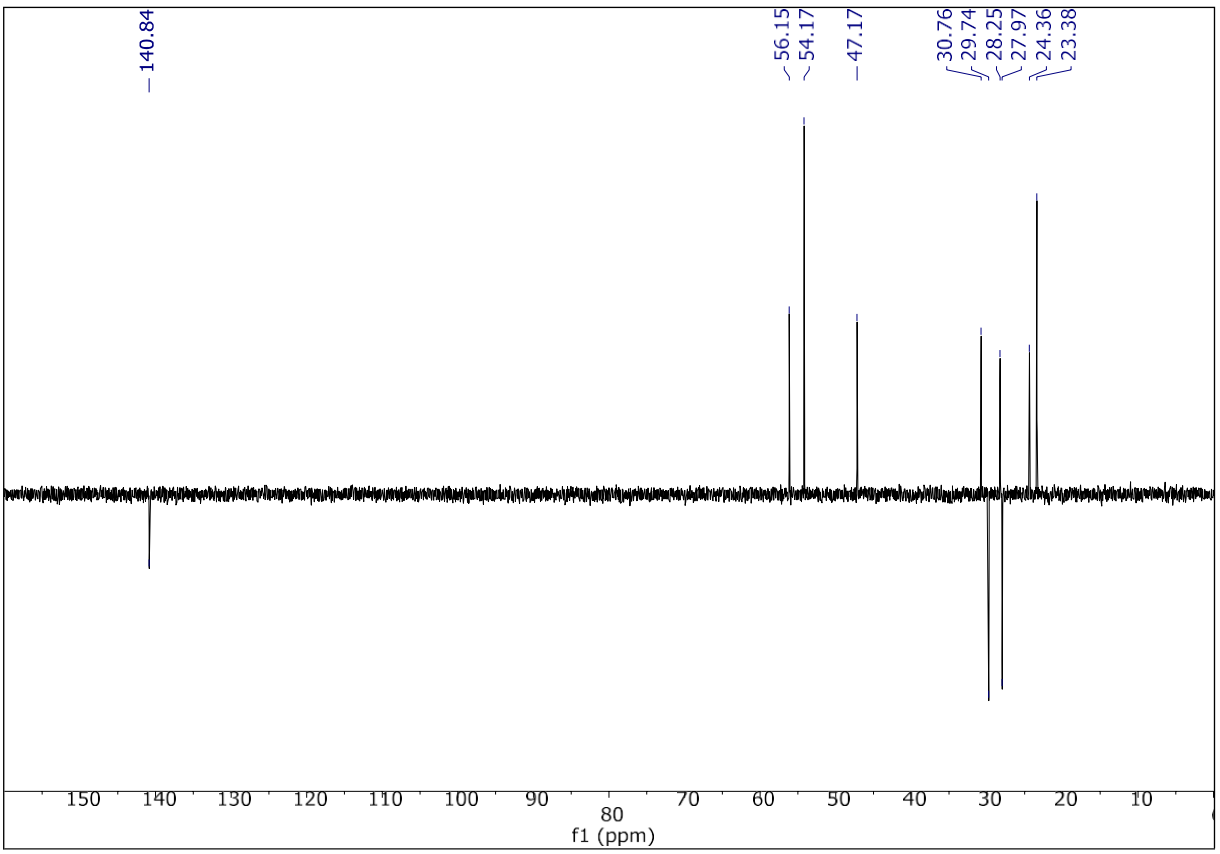

Supplementary Figure S13. ^{1}H NMR (300 MHz) and ^{13}C NMR (75 MHz) spectra in $CDCl_3$ of **10**

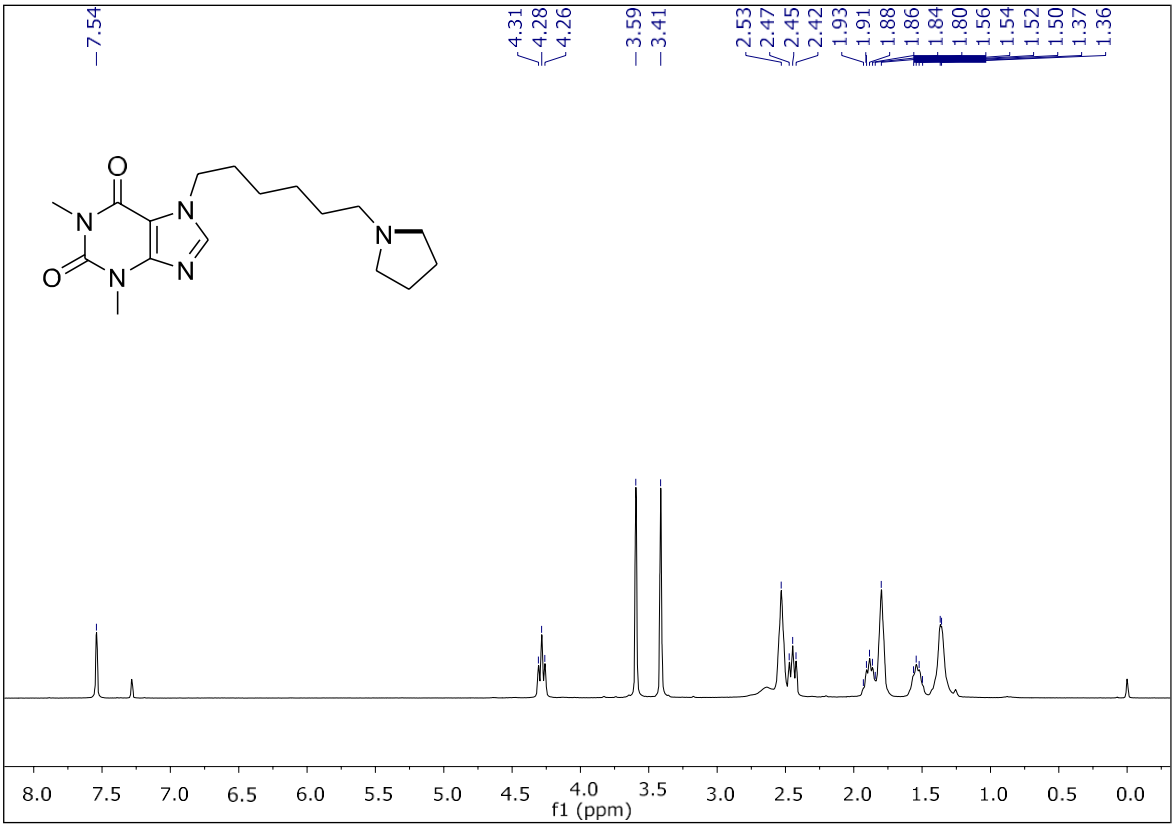

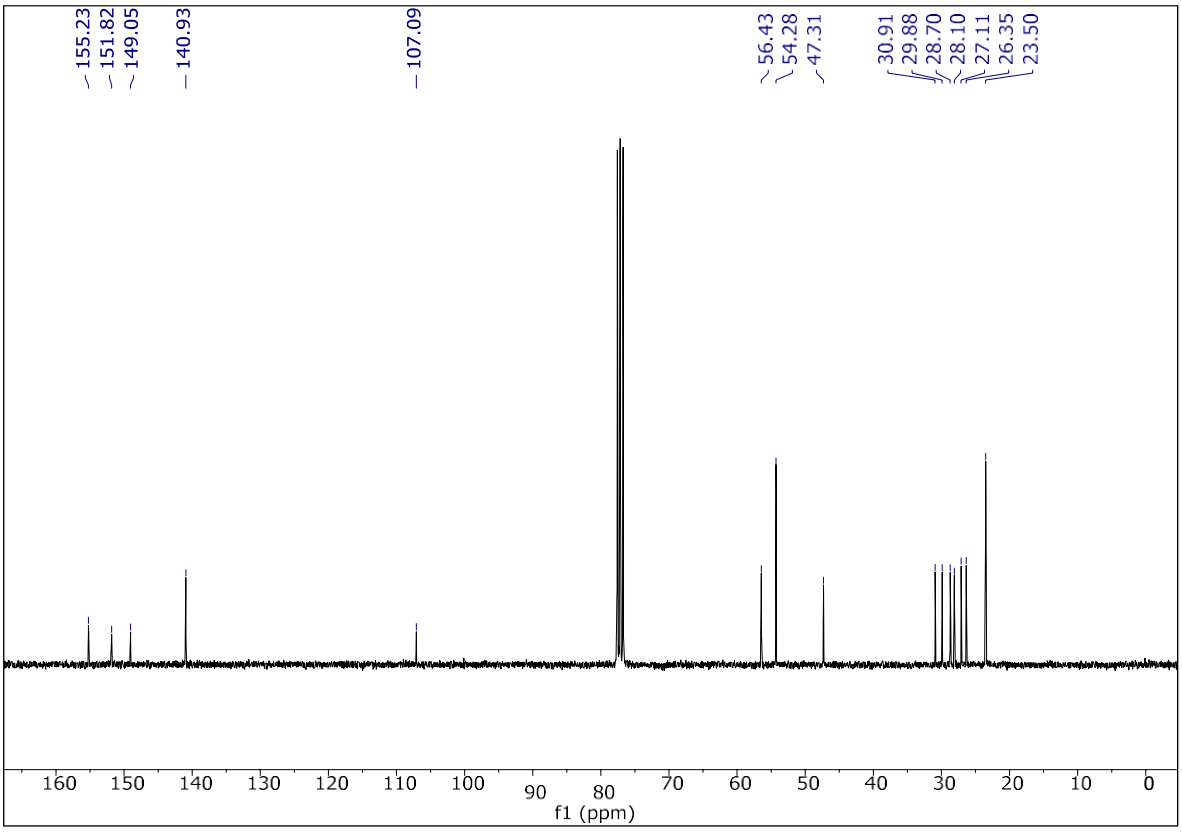

Supplementary Figure S14. HSQC and DEPT spectra in $CDCl_3$ of **10**

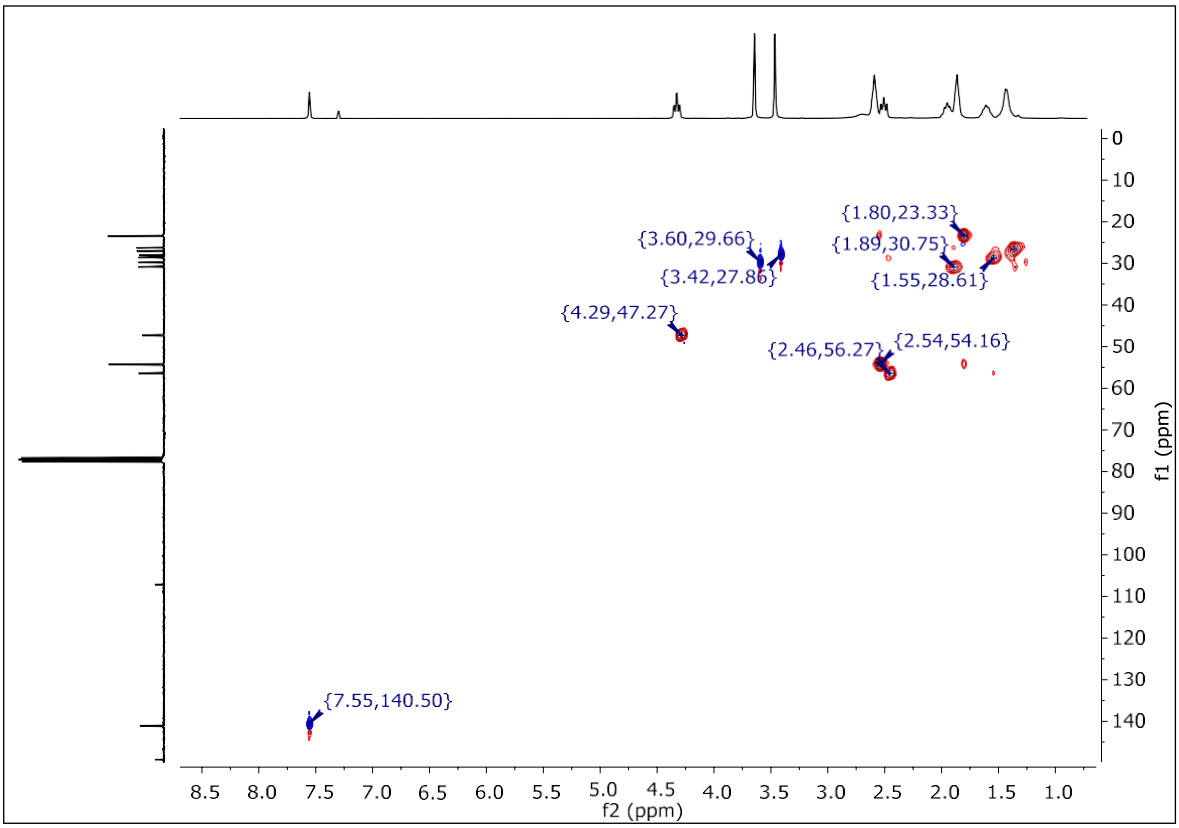

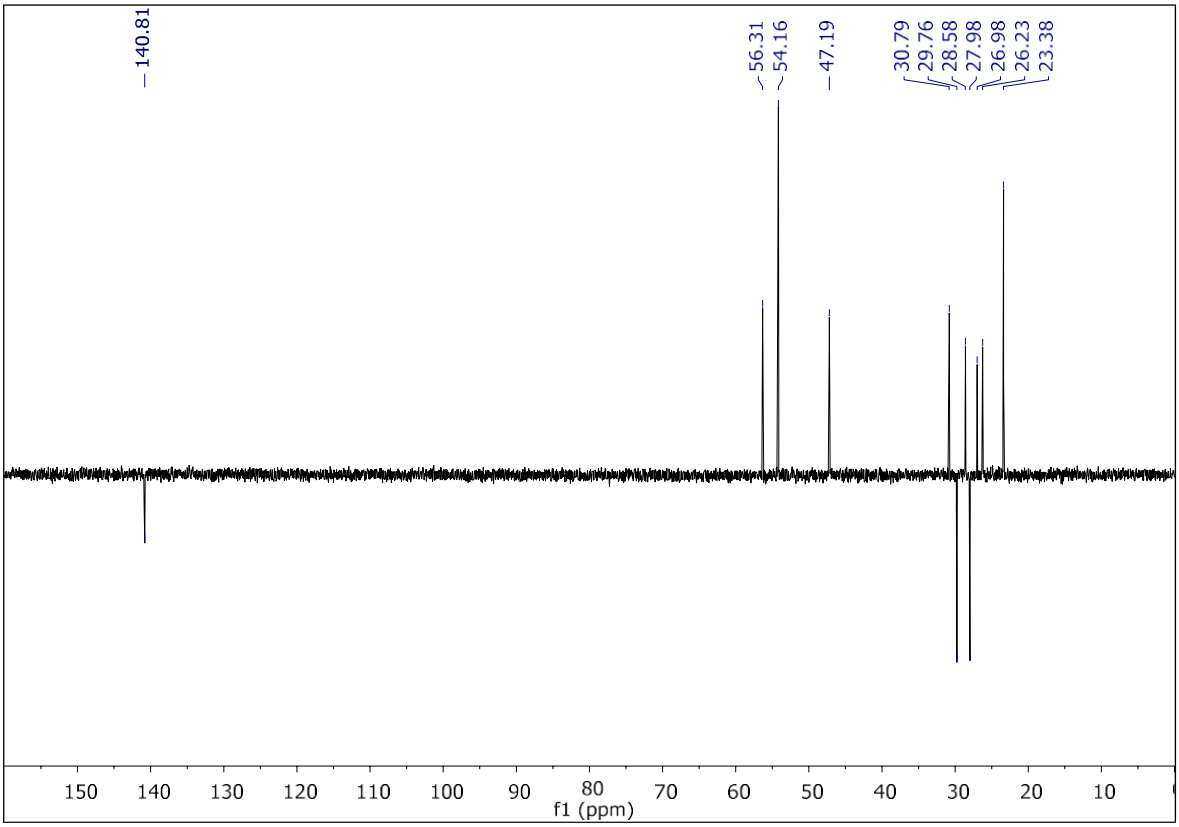

Supplementary Figure S15. ^{1}H NMR (300 MHz) and ^{13}C NMR (75 MHz) spectra in $CDCl_3$ of **11**

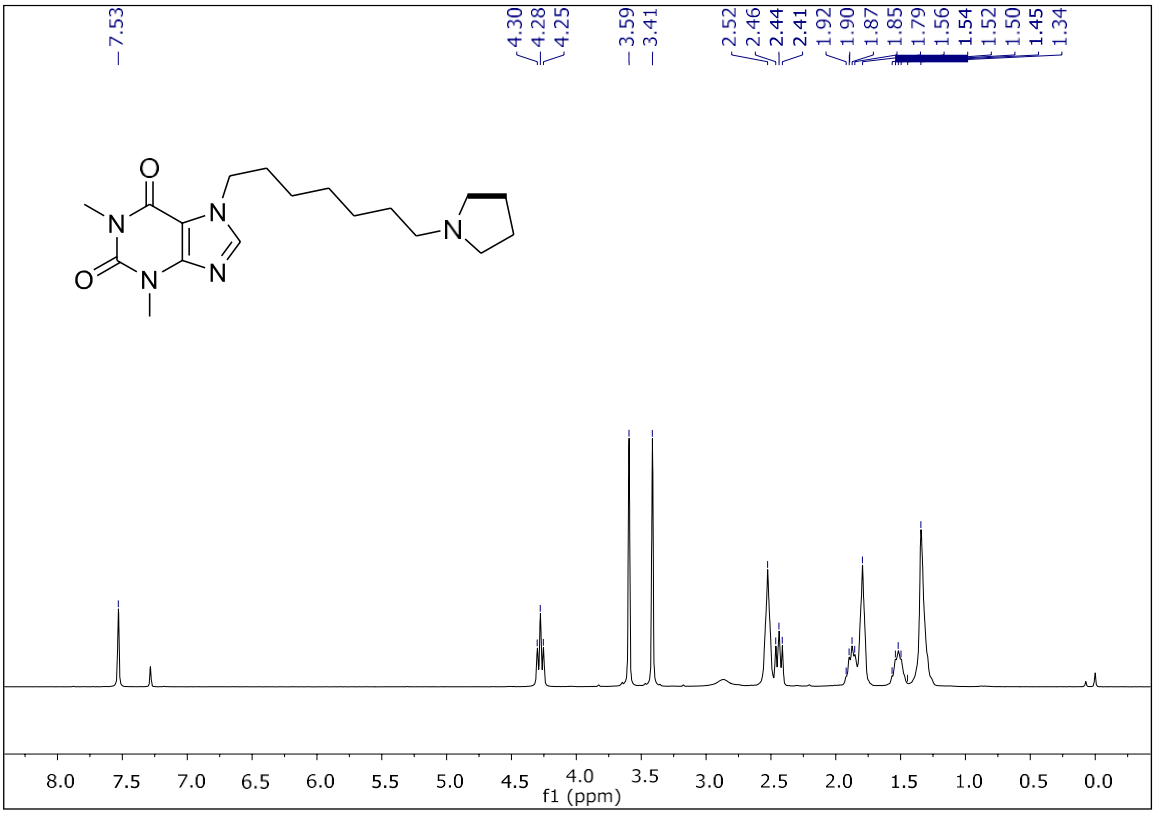

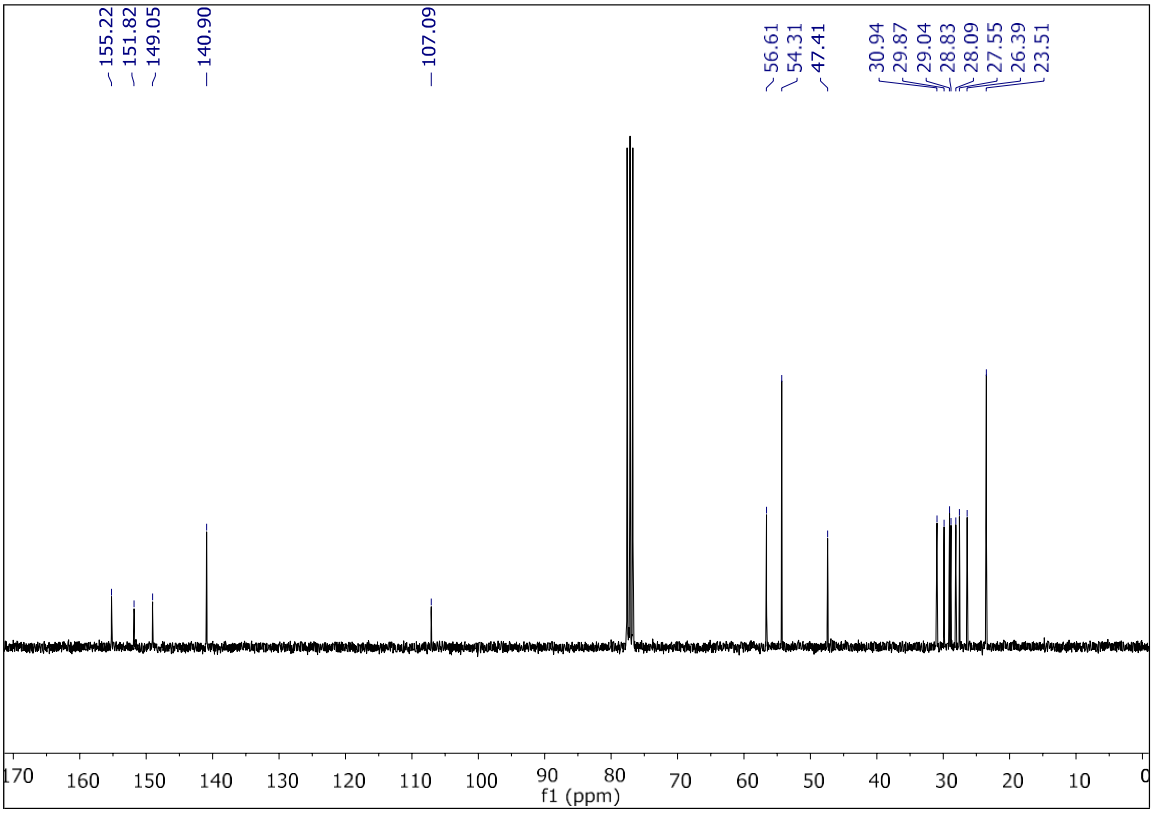

Supplementary Figure S16. DEPT spectra in $CDCl_3$ of **11**